CHAPTER 1

Introduction

1.1 Perception of the Visual World:

The information about the external environment plays a vital role in the survival of any living organism, a primary purpose of life. For example, the detection of the movement of a camouflaging predator under the grass by grazing prey can be crucial for existence. The external environment is a playground for the numerous randomly occurring events, which are multimodal in nature, such as the sound of a thunderstorm, the smell of wet soil, and the visual appearance of lightning. The process of acquiring information about the environment begins with the conversion of the physical input from the external system into neural signals by sensory organs. The ear detects the pressure waves and converts them into neural signals. Similarly, the eye detects the light (photons), the nose detects odor molecules, and the tongue detects particular molecules in food. Humans are thoughtful animals and rely on their sensory organs to explore the environment. However, the sensory organs capture the information in a specific bandlimited range (Figure 1.1). The eye can detect light in the range of wavelengths (400 to 700 nanometers), known as the visible spectrum (Sliney, 2016). On the other hand, human ears are sensitive to the limited frequency range (20 to 20,000 Hertz) of sound waves (Purves et al., 2001).

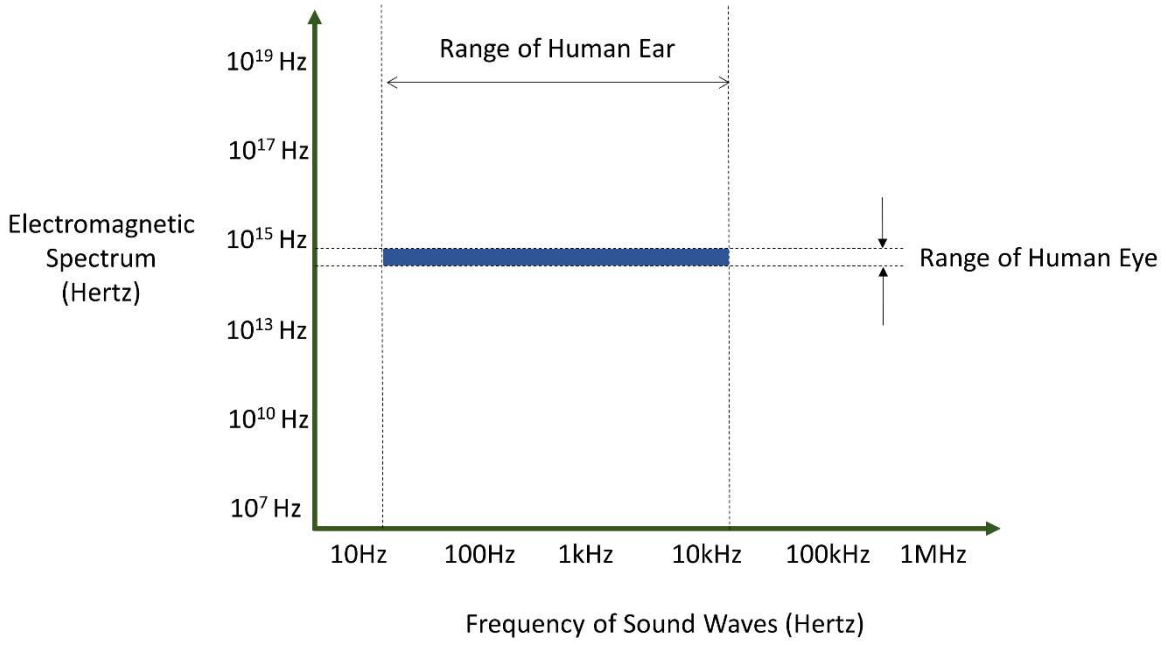

Figure 1.1. Limited detection ranges of the human ear and human eye.

In case of a lesion or absence of a specific sensory organ, the animal cannot get knowledge about the events belonging to that sensory modality. A blind person cannot see the lighting in the sky, and dorylus ants, in which the visual system doesn't exist (Schöning, 2008), are unaware of the visual information. Next, the sensory organs transmit the neural signals to specific brain regions. The brain's neural circuits in the different brain regions organize and process the conveyed signals to extract useful information about the event that occurred in the environment.

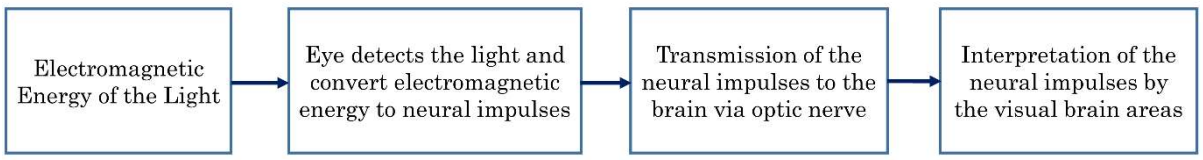

Figure 1.2. The brief outline of the process of visual perception.

The process of identifying and interpreting sensory information is called perception. Perception can be named depending on the sensory system involved, such as visual perception, auditory perception, olfactory perception, and tactile perception. Figure 1.2 outlines the process involved in perceiving a visual event. Perception does not solely depend on sensory information, but various factors, such as attention (Posner et al., 1980; Watanabe and Shimojo, 1998), prior experience (Daelli et al., 2010), memory (Summerfield et al., 2011), and expectation (Puri and Wojciulik, 2008; Matthews and Gheorghiu, 2016), can influence perception. Attention plays a crucial role in visual perception by selectively focusing on specific aspects of the visual scene. The brain filters out irrelevant information and directs attention to what is relevant or salient. This process enabled to prioritize important stimuli and disregard background noise.

Similarly, memory also influences visual perception. Our previous experiences and knowledge shape the perception of the presented visual stimuli. Humans often rely on stored information to recognize objects, faces, and scenes, allowing to interpret the visual input quickly. Interestingly, cultural differences also influence visual perception (Kantner et al., 1968; Kastanakis and Voyer, 2014). Different cultures have unique perceptual biases and preferences, affecting how individuals perceive and interpret visual stimuli. For example, cultural upbringing may influence appreciation for specific colors, patterns, or facial expressions. Hence, perception is a subjective process since the factors influencing the perception can vary from person to person. This dynamic nature of the perception strongly indicates that there might be differences between the physical reality of the environment and the perception of the environment.

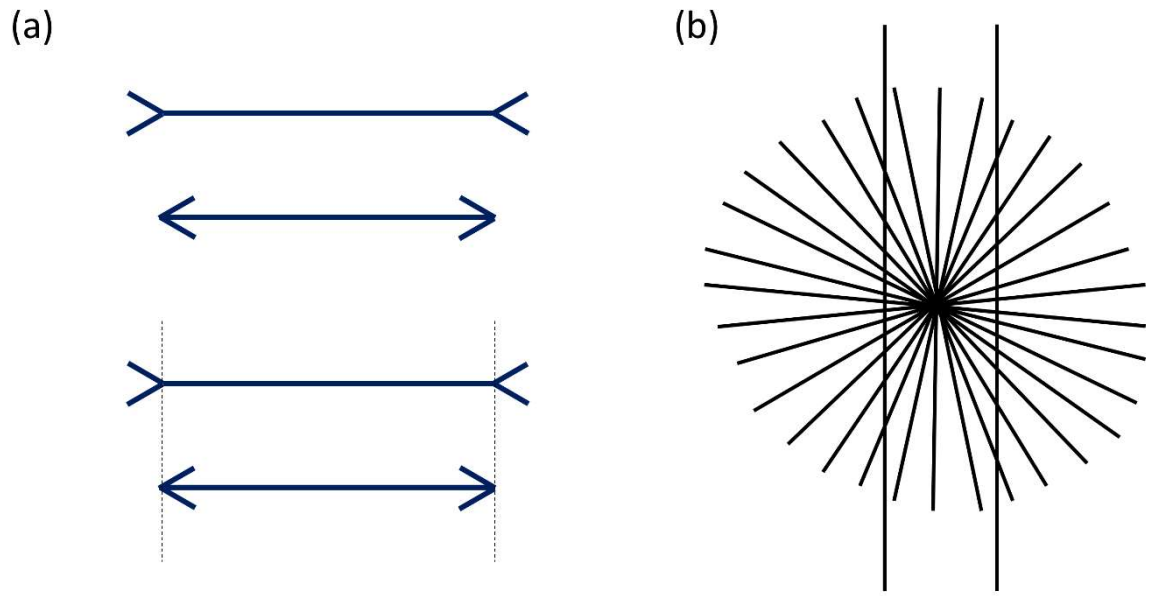

Figure 1.3. The visual illusions show that perception and reality may not be the same. **(a)** The length of the two equal-length lines is perceived as unequal due to the presence of fins in the well-known Müller-Lyer illusion. **(b)** Two parallel lines are perceived as curved in the popular Hering illusion.

The various sensory illusions (Eagleman, 2001; Kelley and Kelley, 2014) are empirical evidences that perception might differ from reality. Two visual illusions are shown in Figure 1.3 as an example. Two straight lines having the same length are perceived as unequal due to the different positions of the fins at both ends in the Müller-Lyer illusion (Berry, 1968) in Figure 1.3(a). Another illusion is in Figure 1.3(b), where the two parallel straight lines are perceived as curved and not parallel, known as the Hering illusion (Hering, 1861). The process of visual perception looks really effortless for the observer compared to other mental tasks, such as thinking or adding two numbers. However, the perception of visual illusions highlights the brain's active endeavor to make sense of sensory information.

Indeed, visual illusions demonstrate how arranging sensory information in a specific way can alter visual perception. Interestingly, two observers may interpret the visual illusions

differently even when presented with identical sensory input. For example, autistic children perceive the Müller-Lyer and rubber hand illusions differently than non-autistic children (Palmer et al., 2013; Manning et al., 2017). Moreover, administering biologically active drugs like ketamine and mefloquine can influence the perceived strength of these visual illusions (Edwards and Cohen, 1961; Gelbtuch et al., 1986; Borruat et al., 2001). Consequently, the process of perception, driven by brain activity, is both dynamic and subjective. The alterations in perceiving the visual illusions under pathological conditions can be used as a non-invasive biomarker for the early detection of neurological disorders (Massironi et al., 1988; Fradkin and Silverstein, 2022; Diez-Cirarda et al., 2023).

Most of the sensory illusions described in the literature are generated by humans and are seldom encountered in natural settings. Nevertheless, the human visual system itself generates certain illusions during the process of visual perception, typically unaware to human observers. For instance, human observers do not feel the boundary of the eyes/retina while observing any visual event, unlike the boundaries of the video recorded by a digital video camera. Similarly, the nose is constantly in the field of view of the eye, but the brain filters the nose out from conscious perception.

1.2 Different factors affecting Visual Perception

Visual perception is a subjective experience influenced by multiple factors associated with the surroundings and the individual observing it. These factors impact how an external event is visually perceived, and these factors are connected to either the observer's external environment or their internal physiological processes. We can classify the various factors that affect visual perception into two main categories: external factors and internal factors. The subsequent subsections will delve into the discussion of few significant internal and external factors.

1.2.1 External Factors

The external factors linked to the properties and processes of the surrounding environment are responsible for influencing how an observer perceives visual information. These factors typically pertain to the physical characteristics of the surroundings. For instance, the presence of other stimuli in the surrounding environment plays a role in modulating and affecting visual perception. These stimuli can interact with the target stimulus and influence various aspects of perception, including contrast detection, brightness perception, and object recognition. Research has provided insights into how the presence of other stimuli can shape visual perception. For instance, studies by Snowden et al. and Xing et al. have shown that the presence of high-contrast stimuli in the environment can impact the ability to accurately detect contrast (Snowden and Hammett, 1998; Xing and Heeger, 2000). The presence of high-contrast stimuli can influence contrast detection thresholds and contrast discrimination, altering the perception of the target stimulus.

Texture interactions between stimuli in the environment have also been found to affect visual perception. Chubb et al. investigated the impact of surrounding textures on the perception of brightness and contrast (Chubb et al., 1989). The findings revealed that the contrast of the surrounding texture in the same spatial frequency range significantly influences the perceived contrast of a textured area. This indicates that the surrounding context of an object can influence the perception of brightness and contrast, highlighting the role of texture interactions in visual perception. Furthermore, the presence of other stimuli can influence object recognition. The phenomenon of "visual crowding" occurs when the presence of nearby stimuli hinders the recognition and identification of a target stimulus. Various studies have observed crowding effects (Bouma, 1970; Pelli et al., 2004), revealing how the presence of nearby stimuli can interfere with the ability to perceive and recognize individual objects. Thus, one can underscore the importance of considering the context and surrounding stimuli when studying and understanding how humans perceive visual information.

The relationship between body size and the size of objects in the environment has been found to have a modulatory effect on visual perception. Research has demonstrated that the relative size of the human body compared to environmental size can influence the perception of the surrounding world. Studies have revealed that children, who have smaller bodies relative to the environment, tend to perceive objects as larger compared to adults (van der Hoort et al., 2011; van der Hoort and Ehrsson, 2014). The observer's body size and developmental factors influence the perception of object size and spatial relationships. The body acts as a reference point or frame of reference that helps calibrate the perception of object size and distance. This phenomenon, can be termed as the body scaling effect, highlights the dynamic interaction between body representation and the perception of the external world. The findings indicate

that the perception of object size is not solely determined by retinal image size but is also influenced by the relationship between body size and the size of objects in the environment.

Lighting conditions or illumination is another factor, that plays a role in modulating visual perception. The amount, quality, and direction of light in the environment can impact the perception and interpretation of visual information. Different research studies demonstrate that bright or dim lighting can alter the perception of colors, shapes, and textures. For example, a study found that changes in illumination affected the perception of surface reflectance and led to color constancy illusions, where the perceived color of an object appeared different under different lighting conditions (Rensink and Cavanagh, 2004). Furthermore, the direction of light can create shadows, which can affect the perception of depth, shape, and texture. Studies have shown that the presence of shadows can enhance the perception of depth and object shape, as shadows provide valuable cues for interpreting three-dimensional structures (Mamassian and Goutcher, 2001). Additionally, the quality of light, such as natural sunlight versus artificial lighting, can also influence visual perception. For instance, exposure to different light spectra influences visual acuity, alertness, and mood, suggesting that the spectral composition of light can impact various aspects of visual perception and cognitive functioning (Askaripoor et al., 2019). Therefore, lighting conditions are an important environmental factor that can modulate visual perception, affecting the perception of colors, depth, shape, and overall visual experience.

One of the most important factors is motion which plays a crucial role in modulating and influencing visual perception. The presence of motion in the visual scene provides dynamic information that affects the interpretation of objects, depth, spatial relationships, attention, and visual stability. Motion has a profound impact on the perception of object

properties. The perception of object contours can be influenced by the movement of surrounding elements, and motion cues can enhance or disrupt the perception of object form (Reuter-Lorenz et al., 1996). Additionally, the perceived shape of an object can change based on the direction and speed of motion, revealing the dynamic nature of object perception (Giese and Poggio, 2003; Tse and Hsieh, 2006). The above mentioned findings highlight the role of motion in shaping the perception of object structure and form.

Moving stimuli tend to capture and direct attention more effectively than static stimuli. The presence of motion in a scene can modulate our attentional focus, influencing the perception and processing of visual information. Motion information can attract and guide attention toward relevant objects in a scene, facilitating faster and more efficient visual search (Wolfe, 1994). Moreover, the perception of stationary objects can be influenced by the motion of surrounding elements, leading to phenomena such as motion-induced blindness, where stationary objects briefly disappear from our conscious perception (Bonneh et al., 2001). These findings demonstrate the intricate relationship between motion and attention, highlighting the role of motion in guiding visual focus. Despite continuous eye movements, perception of the external world remains relatively stable. Motion signals play a crucial role in compensating for the retinal image changes induced by eye movements, allowing for the perception of a coherent visual scene. Studies have investigated mechanisms such as corollary discharge and efference copy to understand how the brain achieves visual stability in the presence of motion (Wurtz, 2008). By integrating motion signals, the visual system can maintain a stable perception of the world despite the eye movements.

One intriguing phenomenon related to motion and perceived length is motion-induced compression. When a stationary line is presented alongside a moving line of the same physical

length, the moving line appears compressed in the direction of motion. This compression effect is thought to result from the integration of motion signals and spatial information within the visual system. An influential study by Nijhawan demonstrated the effect, suggesting that motion signals can alter the perceived length (Nijhawan, 1994). The motion-induced compression phenomenon highlights the dynamic nature of visual perception and how motion cues can influence our perception of length. The integration process may occur at various stages of visual processing, involving interactions between motion-sensitive neurons and spatial processing pathways. The precise mechanisms underlying the integration of motion and length are still a topic of ongoing research. However, neuroimaging studies have provided insights into the neural correlates of motion-induced length distortions, indicating the involvement of cortical regions such as the motion-sensitive areas (Muckli et al., 2005).

Perceived velocity refers to the subjective experience of an object's speed or motion. While physical velocity is determined by an object's displacement over time, the perception of velocity can be influenced by various factors. For example, the perception of velocity can be influenced by the surrounding context in which the object moves. When an object moves against a complex background, its perceived velocity tends to differ from when the object moves against a simple background (Thompson, 1982). This phenomenon highlights the impact of contextual cues on velocity perception.

Motion perception is a critical aspect of human visual function, especially in activities such as driving, where accurate perception of moving objects and surroundings is essential for safety. The influence of lighting conditions on motion perception has been a subject of research. Elderly drivers often encounter disability-inducing glare at night from the headlights of oncoming vehicles (Anderson and Holliday, 1995). Experiments conducted to assess the

effect of glare from vehicle headlights on visual performance revealed significant implications for seeing moving targets under differing lighting conditions. Mimicking age-induced eye cataracts simulated lens opacities, which have little effect on standard daytime visual acuity, markedly affected night time contrast sensitivity for moving targets. High-beam glare, in particular, was found to reduce maximum contrast sensitivity by an order of magnitude in individuals with mild lens opacities (i.e. cataracts) or people who have night vision difficulty due to nutritional deficiency as vitamin A. These findings underscore the importance of considering the impact of glare and lighting conditions on visual performance, especially for vulnerable populations like elderly drivers.

A study has been aimed to determine the impact of glare, simulating the effects of oncoming vehicle headlights, vis-à-vis aging visual changes on different aspects of motion perception (Sepulveda et al., 2022). The research involved younger and older visually healthy adults completing various visual motion tasks under glare and no-glare conditions. While older adults exhibited increased intraocular starlight and elevated thresholds for some motion perception tasks compared to younger adults, it was found that glare did not further elevate these thresholds. These results suggest that while age-related changes in vision can affect motion perception, glare from off-axis light sources may not exacerbate these effects.

A study has shown that drivers are more likely to be involved in collisions during the night than during the day (Kim, 2015). Research were targeted to investigate whether differences in light levels between day and night periods affect the drivers' perceptions of speed on rural roads. Experiments revealed that while participants were sensitive to small differences in egocentric speed under different lighting conditions, light levels did not significantly impact

their perceptions of speed. However, participants tended to underestimate their absolute speed, indicating potential challenges in accurately judging speed regardless of lighting conditions.

The effect of lighting on motion perception is complex and multifaceted, influenced by factors such as glare, age, and individual physiological and personality differences. While glare from vehicle headlights can significantly impact visual performance, especially in night time driving scenarios, its effects on motion perception may vary depending on factors such as age, neuropsychological tone and task complexity.

Motion perception is a fundamental aspect of human vision, critical for navigating through the environment and interpreting dynamic visual scenes. However, the perception of motion can be influenced by the presence of noise in the visual stimulus. Using a two-interval forced-choice procedure, a study (Zanker and Braddick, 1999) investigated the assessment of speed in random-dot kinematograms containing different proportions of noise and found that there was no strong reduction in perceived speed with increasing noise levels, as long as coherence levels remained above thresholds for directional judgments. This suggests a considerable but not perfect segregation of signal and noise motion components in the pooling process leading to speed estimation.

Another study (Chuang et al., 2016) investigated how a background stimulus that did not move in a net direction did influenced the perceived speed of a center stimulus. Participants observed two overlapping random-dot patterns, with the center stimulus moving coherently in a fixed direction while the background stimulus moved randomly. Surprisingly, the study found that human subjects perceived the speed of the center stimulus to be significantly faster than its veridical speed when the background contained motion noise. Moreover, the perceived speed was tuned to the noise level of the background, with the highest perceived speed reached

at progressively higher background noise levels as the center speed increased. In conclusion, the perception of motion speed is substantially influenced by the presence of noise.

Understanding how we perceive motion amidst multiple moving objects is pivotal for navigating our surroundings. Research has shown that there is a limit to how many motion signals we can process simultaneously (Edwards and Rideaux, 2013). However, this limit is not universal and depends on factors like signal clarity and background noise. For example, while previous studies suggested a maximum of three perceivable motion signals, recent research using localized stimuli found that the limit could be higher under certain conditions (Alvarez and Franconeri, 2007).

Moreover, the ability to track and attend to multiple moving objects improves with maturity and developmental age (Stubbert et al., 2023). A study involving children and adolescents found that performance on tasks requiring the tracking of moving objects and perceiving biological motion gets better as kids grow older. This indicates that the visual attention skills for tasks like tracking objects or understanding movements of other people continue to develop through childhood into adolescence. In nutshell, the perception of motion is significantly impacted by the number of moving objects in the visual scene.

1.2.2 Internal Factors

Visual perception is a complex cognitive process that interprets and makes sense of visual information. While external stimuli play a pivotal role in visual perception, numerous internal factors encompassing physiological processes, cognitive mechanisms, and individual differences significantly influence how a human observer perceives the visible world.

Understanding internal factors is crucial for unraveling the intricate interplay between the brain and the external environment, shedding light on the fascinating complexities of human perception.

One of the internal factors that can affect visual perception is sensory adaptation. Sensory adaptation refers to the process in which sensory receptors become less responsive to a constant stimulus over time, leading to perceptual alterations. This phenomenon occurs due to the neural mechanisms involved in maintaining the sensitivity of sensory systems. For instance, prolonged exposure to a bright light source can cause visual adaptation, resulting in a dimming of the light's intensity or changes in color perception (Hurvich, 1981). Sensory adaptation showcases the brain's remarkable ability to adjust sensitivity to prevailing sensory information and to process new stimuli efficiently.

Expectations and beliefs significantly impact visual perception. Preconceived notions and stored knowledge shape how the observer will interpret sensory information, often leading to alterations in visual perception. These expectations can arise from past experiences, cultural influences, or cognitive biases. Research has shown that expectations can modulate neural activity in early visual areas, influencing perceptual processing (Summerfield and Egner, 2009). For example, suppose an observer expects to see a familiar face in a crowd. In that case, the human brain may interpret ambiguous visual stimuli as resembling that face, demonstrating the power of expectations in shaping perception. Additionally, beliefs and cultural influences can lead to perceptual biases, as different cultures may have varying perceptual priors and interpretive frameworks (Nisbett and Masuda, 2003).

Emotions play a profound role in influencing visual perception. Emotional states can bias the interpretation of visual information, leading to altered perception. Emotions can

enhance or diminish the salience of specific stimuli, influencing attentional focus and perceptual processing. Fear, for instance, can heighten vigilance and magnify the perception of threatening stimuli, even when the actual threat level is low (Vuilleumier, 2005). Similarly, positive emotions such as happiness can influence the perception of pleasant or rewarding stimuli. The emotional context in which we perceive the visual world adds another layer of complexity to the perceptual experiences and can influence the allocation of attentional resources and the interpretation of visual information (Wadlinger and Isaacowitz, 2006; Gable and Harmon-Jones, 2010; Wyczesany et al., 2018; Niedenthal and Wood, 2019). Deeply ingrained in human thinking patterns, cognitive biases influence how an observer perceives the world visually. Cognitive biases stem from mental shortcuts and heuristics that streamline information processing but can introduce distortions in visual perception. Take confirmation bias, for instance, which subtly molds the interpretation of visual stimuli to align with existing beliefs, potentially warping the understanding of reality (Wolfe et al., 2005; Rajsic et al., 2015; Walenchok et al., 2020).

The way a human observer perceives visual stimuli varies among individuals, shaped by a complex interplay of cognitive abilities, attentional capacity, age, and past experiences. Each person brings a unique combination of factors, resulting in diverse interpretations of the same visual information. These discrepancies can be attributed to various factors, including the efficiency of neural processing, the control of attention, and the integration of prior knowledge. Fascinatingly, research has shown that age-related changes in visual perception can significantly impact the processing of visual information, particularly in tasks that require a considerable amount of attentional resources (Faubert, 2002; Brennan et al., 2017; Meng et al., 2019). Moreover, individuals with expertise in specific domains, such as artists or

scientists, may exhibit exceptional perceptual abilities due to their extensive training and domain-specific knowledge (Mulas et al., 2012).

The influence of biochemical, pharmaceuticals, or neuromodulatory agents on visual perception is an area of great interest, as various substances can significantly alter our visual experiences. Some biochemicals can directly affect the neural processes involved in visual perception, leading to distortions, illusion, deformation, or changes in visual acuity. Substances such as LSD (lysergic acid diethylamide), psilocybin (found in certain mushrooms), and mescaline (from peyote cactus) are known for their visual confounding. These drugs can profoundly alter visual perception, leading to vivid and intense visual deformation. Users may experience distorted shapes, colors, patterns, or even perceive objects that are not present. The illusory effects are thought to result from interactions with serotonin receptors in the visual cortex, disrupting normal neural processing and producing perceptual distortions (Hasler et al., 2004; Carhart-Harris and Nutt, 2017).

Neuromodulators like amphetamines, caffeine, and MDMA can modulate visual perception by increasing arousal, attention, and altering the release of neurotransmitters such as dopamine and norepinephrine. These substances can enhance visual acuity, intensify colors, and lead to heightened sensitivity to visual stimuli. Users may experience increased focus and heightened appreciation of visual details, leading to an enhanced visual experience (Kojima et al., 1986; Vollenweider and Kometer, 2010; White et al., 2013a). On the other hand neuromodulating depressant drugs, such as alcohol, benzodiazepines, and opioids, can have a suppressive effect on visual perception. These substances can slow down neural activity, impair cognitive processing, and lead to blurred vision or diminished visual clarity. Alcohol, for instance, can impair depth perception and visual coordination, making it difficult to judge

distances or perceive fine details, as for instance during driving (Sullivan et al., 1995; Wegner and Fahle, 1999; Wang et al., 2021).

Cannabinol can have variable effects on visual perception depending on the individual and the specific vehicle of this phytochemical used. While some users report enhanced visual experiences, such as intensified colors or heightened visual creativity, others may experience perceptual distortions, such as altered depth perception or slowed visual processing. The effects of cannabinol on visual perception may be mediated by the interaction of cannabinoids with the endocannabinoid system in the brain (Winton-Brown et al., 2011; Ortiz-Peregrina et al., 2021). It is important to note that the effects of neuromodulators on visual perception can vary widely depending on several factors, including the dosage, purity of the substance, individual tolerance, and the presence of other substances in the body. Moreover, the use of neuromodulators can have both short-term and long-term impacts on visual perception and overall cognitive functioning.

The effect of Autism Spectrum Disorder (ASD) on motion perception has been a topic of significant research interest, revealing intriguing insights into the neural mechanisms underlying this condition. Regarding potential with ASD, several studies have investigated the neural responses to motion perception of moving biological objects ("biological motion") (Kaiser et al., 2010). Functional magnetic resonance imaging (fMRI) study have identified three key neural signatures: state activity, trait activity, and compensatory activity. State activity reflects the disruptions specific to individuals with ASD, trait activity indicates shared dysfunction between unaffected siblings and individuals with ASD, while compensatory activity suggests neural mechanisms through which unaffected siblings may compensate for an increased genetic risk (Kaiser et al., 2010).

Moreover, research has delved into the processing of biological motion tasks in individuals with ASD, revealing diverse results. While some studies initially suggested deficits in visual sensitivity to coherent motion but not to point-light displays of human motion, more recent evidence questions this, indicating differences in sensitivity to human motion (Kaiser and Shiffrar, 2009). These findings highlight the complexity of motion perception in ASD and the need to develop a comprehensive understanding of visual perceptual differences in ASD.

In a functional MRI study comparing individuals with ASD to typically maturing and developing individuals, differences in neuronal activation during biological motion perception were observed, along with variations in reaction times (RT) (Kaiser and Shiffrar, 2009). These differences were further associated with imitation, gross motor abilities, and behavioral measures, suggesting a potential link between impaired motion perception and difficulties in imitation and gross motor skills characteristic of ASD (Kaiser and Shiffrar, 2009). Additionally, correlations with gray matter volume and psychopathological measures emphasize the involvement of specific brain regions, such as the parietal cortex and medial temporal cortex, in motion perception deficits and repetitive behaviors in ASD (Kaiser and Shiffrar, 2009). Overall, the research on the effect of ASD disorder on motion perception underscores the complexity of this condition and its impact on various cognitive and perceptual processes.

Attention-deficit/hyperactivity disorder (ADHD) is a neurodevelopmental condition characterized by impairments in attention, hyperactivity, and impulsivity. While traditionally studied in the context of cognitive control and executive functioning, recent research has explored the impact of ADHD on motion perception, shedding light on the neural mechanisms underlying this aspect of the disorder.

Studies investigating biological motion processing in ADHD have revealed alterations in neuronal activity and perception of human motion cues (Kröger et al., 2014; Tian et al., 2024). EEG studies have shown decreased N200 amplitude (the 200 milliseconds negative voltage signal) , a marker of early visual processing, in response to both scrambled and biological motion in individuals with ADHD (Kröger et al., 2014). Furthermore, spatio-temporal analysis demonstrated reduced and more diffuse activation in occipital-temporal regions during human motion processing in ADHD subjects, indicating neuronal determinants of altered motion processing (Kröger et al., 2014). These findings suggest disruptions in the neural mechanisms underlying the perception of biological motion in ADHD, highlighting the importance of investigating social cognition markers and alteration of biological motion perception, in the context of ADHD.

Moreover, research comparing the abilities to the process local kinematic and global configurational cues, fundamental to biological motion perception, between typically developing (TD) and ADHD children, revealed atypical biological motion perception in ADHD (Tian et al., 2024). Children with ADHD exhibited potential dissociation between local and global biological motion processing, with local processing ability being significantly related to social interaction skills (Tian et al., 2024). Additionally, the sustained attention ability significantly influenced general biological motion perception in ADHD children, mediated by reasoning intelligence (Tian et al., 2024). These findings underscore the intricate relationship between motion perception deficits and core symptoms of ADHD, such as impaired social interaction and attentional difficulties.

Furthermore, studies investigating the effects of ADHD on driving behavior, utilizing a driving simulator with visual motion cues, demonstrated differences in speed perception and

regulation between individuals with ADHD and typically developing subjects (Lidestam and Thorslund, 2019). ADHD drivers exhibited less sensitivity to extra motion cues and were less inclined to adjust their speed between replicates compared to controls, suggesting a rule-based approach to speed perception driven by attentional factors (Lidestam and Thorslund, 2019). These findings highlight the potential implications of motion perception deficits in real-world tasks, such as driving, in individuals with ADHD.

Additionally, there has been performed further research contrasting cognitive control and error processing during tasks with static visual forms and moving random dot patterns; the studies revealed deficits in performance and brain activity in children with ADHD, particularly for moving stimuli (Lange-Malecki et al., 2018). The ADHD group showed decreased accuracy and prolonged response times for both static and moving stimuli, indicating a higher-order cognitive control deficit independent of stimulus type (Lange-Malecki et al., 2018). These findings emphasize the importance of considering motion processing deficits in the broader context of ADHD-related cognitive impairments. In conclusion, recent research has provided convincing evidence for alterations of motion perception in individuals with ADHD, shedding light on the neural mechanisms underlying this aspect of the disorder.

Schizophrenia, a complex mental disorder characterized by impairments in perception, cognition, and social functioning, has been associated with deficits in motion perception, which play a crucial role in social interaction and everyday activities. Recent research has provided insights into the effect of schizophrenia on motion perception, highlighting alterations in both behavioural and neural responses to visual motion stimuli.

One study investigated the discrimination of small velocity differences in patients with schizophrenia, revealing impairments in contrast sensitivity related to motion perception (Chen

et al., 1999). The study utilized a motion discrimination task and found that schizophrenic patients exhibited lower contrast sensitivity than controls when detecting small velocity differences between moving stimuli (Chen et al., 1999). This impairment suggests difficulties in processing motion signals, potentially stemming from alterations in the neural systems responsible for motion perception.

Furthermore, research employing a biological motion paradigm demonstrated deficits in biological motion perception in schizophrenia patients, particularly when perceptual signals were moderately degraded by noise (Kim et al., 2013a). Schizophrenia patients exhibited lower accuracy in the biological motion perception task compared to healthy controls under conditions of moderate signal degradation (Kim et al., 2013a). This deficiency in processing biological motion information indicates disruptions in the integration of basic visual motion signals, emphasizing the importance of addressing visual motion perception deficits in social cognitive remediation interventions for schizophrenia.

Additionally, electroencephalography (EEG) studies have provided insights into the neural correlates of impaired biological motion perception in schizophrenia (Jahshan et al., 2015). Schizophrenia subjects showed reduced recognition of biological motion stimuli compared to healthy controls, accompanied by alterations in neural responses during visual processing (Jahshan et al., 2015). While early visual processing stages were not significantly affected, schizophrenia subjects exhibited dysfunction in later stages, indicating difficulties in long term identification of human form in biological motion stimuli (Jahshan et al., 2015).

A systematic review and meta-analysis further confirmed abnormalities in biological motion perception in schizophrenia patients across multiple studies (Okruszek and Pilecka, 2017). The meta-analysis revealed reduced biological motion processing capacity in

schizophrenia patients compared to healthy controls, with significant effects observed in both general and specific biological motion-based tasks (Okruszek and Pilecka, 2017). These findings underscore the consistent evidence for deficits in biological motion perception in schizophrenia and reiterates the importance of addressing these impairments in clinical assessments and interventions. Schizophrenia is associated with impairments in motion perception, as evidenced by deficits in discriminating velocity differences, processing biological motion stimuli, and neural responses during visual processing.

Depression, a prevalent mental health condition with the largest prevalent worldwide, is characterized by persistent feelings of sadness and loss of interest, and has been associated with alterations in visual perception, including motion processing. Recent research has shed light on the effect of depression on motion perception, highlighting dysfunctionality in inhibitory processes and global motion processing.

Studies have revealed depleted concentrations of inhibitory neurotransmitter in the occipital cortex of individuals with depression, suggesting weakened inhibition within their visual systems (Golomb et al., 2009b). To explore this further, researchers examined the inhibitory process of centre-surround suppression of visual motion in depressed individuals (Golomb et al., 2009b). Results indicated alterations in center-surround suppression in depression, modulated by stimulus conditions such as contrast, size, and presentation time (Golomb et al., 2009b).

Moreover, the investigations analyzing global motion processing in depression has shown abnormalities in inhibitory processes within this domain (Norton et al., 2016). Depressed participants displayed reduced global center-surround suppression effects compared to controls, particularly in unmedicated individuals (Norton et al., 2016). Alterations in centre-

surround suppression effects suggest dysregulation of inhibitory processes specific to motion perception in depression (Norton et al., 2016). Depression is associated with abnormalities in motion perception, including deficits in inhibitory processes and motion processing. These findings incisively contribute to our understanding of the visual system's dysregulation in depression and underscore the importance of considering motion perception deficits in the assessment and treatment of depression.

1.3 Objectives of the Current Investigations:

Our investigations are driven by the primary objective of developing a quantitative and computational model that captures the alterations occurring in visual perception. As mentioned in section 1.2, visual perception is a dynamic process influenced by various factors. While it would be ideal to consider all known factors, the complexity of human perception makes it almost impossible to address them all. Therefore, we have chosen to focus on important factors: the activation of the sympathetic or parasympathetic nervous system (an internal factor), and the movement of objects (an external factor).

Let us consider the aspect of internal factor (sympathetic/parapathetic nervous system activation). The human brain responds to external and internal stimuli by activating either the sympathetic or parasympathetic nervous system, which is crucial for survival. It is already established that the activation of these systems can impact visual perception—an internal factor, as reported by Fischer (Fischer, 1971). However, only a very few experiments have effectively measured the effects of nervous system activation on functions related to visual perception. A quantitative framework capable of assessing these modulatory effects is still

lacking. Our objective is to develop a quantitative framework that captures the variations in visual perceptual functions as there is an alteration of sympathetic or parasympathetic nervous system activity. To achieve this, we have chosen to alter the dosage amount of drugs or neuro-pharmaceuticals so as to induce varying levels of sympathetic or parasympathetic activity. Our primary goal, therefore, is to develop a mathematical model that represents the relationship between drug dosage (indicative of nervous system activation) and alterations in visual perception. We will validate our model using experimental behavioral data. Additionally, we aim to formulate a framework for understanding the neuronal-level processes responsible for the alterations in visual perception. Finally, we will develop a computational model of the neural circuits and conduct a neuroimaging experiment to verify our proposed framework. **Chapter 2** provides detailed elucidation of our quantitative framework, methods, and results.

We now come to the consideration of our external factor (movement of the object). Perceiving moving objects is an important aspect of visual perception. As objects move, spatial positions change over time. Consequently, perceiving moving objects involves combining information from both spatial perception and temporal perception. As previously discussed in section 1.2.1, motion—an external factor—can influence visual perception. In this study, our primary objective is to establish a mathematical framework that quantifies the variations in spatial perception and temporal perception resulting from an object's motion so that there is maintained the same temporal causality relationship (i.e. order of events) in both physical space and perceptual space. We have validated our mathematical framework using experimental behavioral data. Additionally, we aim to identify potential anatomical sites and formulate the underlying neuronal mechanisms responsible for the modulation of spatial and temporal perception due to object movement. To further verify our framework, we have conducted

neuroimaging experimentation. Detailed descriptions of our mathematical model, experimental validation, and results are provided in **Chapter 3**.

CHAPTER 2

Alterations in Visual-Spatial Perception due to change in Autonomic Nervous System Activation

2.1 Introduction:

The sensory system in the human body transmits information about the surroundings to the nervous system. The brain organizes and interprets this information in the collective process termed as perception. Perception creates an internal map of the outside world and significantly impacts everyday life. For instance, the color red is a specific wavelength of electromagnetic radiation, but perceptually mapped as a visual property. Its presence can psychologically affect decision-making (Elliot et al., 2007). Perceiving an external event is a complex process influenced by various factors beyond sensory information. For example, in the case of the Ponzo illusion, the perceived length of the two physically equal straight lines is unequal because of the contextual information (Ponzo, 1911). Different types of sensory illusions, such as tactile, auditory, olfactory, and visual illusions, demonstrate that the perception of the environment can differ from reality because of how sensory information is organized (Ponzo, 1911; Eagleman, 2001; Kalderon, 2011; Lederman and Jones, 2011; Stevenson, 2011). However, even if the surrounding environment is the same, a person can perceive sensory illusions differently if the biochemical activity in the brain is modulated or modified due to any endogenous or exogenous factor (Van Loon et al., 2013; Costa et al., 2021). One such factor is the arousal or activation of the autonomic nervous system, which

influences the biochemical activity in the brain and thus can alter the perception of the external environment.

The autonomic nervous system regulates the physiological response to immediate stress by the "fight-or-flight" response, referred to as hyperactivation. Reciprocally, a "rest-and-digest" state facilitates relaxation and recovery, referred to as hypoactivation (McCorry, 2007). Hyperactivation and hypoactivation may not necessarily occur in response to an external hazard, but they can also occur due to other factors such as neurochemical or neuromodulator action or stimulus. Hyperactivation and hypoactivation are associated with the actuation of the sympathetic and parasympathetic nervous systems, respectively. Indeed, hyperactivation and hypoactivation of the autonomic nervous system cause perceptual variations and distortions in the visual perspective, handwriting area, finger tapping rate, taste threshold, brightness sensitivity, etc (Fischer, 1971).

Several factors can induce the alteration of the activation level. Nevertheless, biochemical alterations of arousal due to an oral dose of a neuromodulator agent in an experimental setting are more convenient for mathematical modeling of the activation level. Examples of hyperactivation state-inducing neuromodulating agents include tryptamine-derivatives, glycolate, psilocybin, and adrenochrome. Conversely, hypoactivation state-inducing neuromodulating agents encompass phenothiazine-derivatives, dextomid, chlorpromazine, and alimemazine. The two groups of neuromodulating agents act by activating the sympathetic and parasympathetic nervous systems, respectively. When administered, such agents cross the blood-brain barrier, diffuse in the brain's extracellular space, and produce pharmacological and biological activity (Pardridge, 2012).

Autonomic nervous system activity has been the focus of various studies which observed the corresponding impact on visual perception. For instance, research has indicated that the Mueller-Lyer illusion, a well-known visual illusion, was modified by neurochemically-induced sympathetic nervous system activity (Edwards and Cohen, 1961; Olbrich et al., 2021). Another study found an association between psilocybin-induced sympathetic nervous system activity and change in the handwriting area, an indication of alteration in visual-spatial perception (Fischer et al., 1969b). Moreover, alterations in brightness preference (Fischer et al., 1969a) and visual-motion perception (Carter et al., 2004) were observed due to the change in activity of the sympathetic nervous system as modulated by the psilocybin action. On the other hand, the activity of the parasympathetic nervous system also affects visual perception. The chlorpromazine-induced parasympathetic nervous system alters the spatial distortion threshold, a direct manifestation of the corresponding alteration in visual perception (Hill and Fischer, 1971a). Despite the experimental observations of the changes in visual perception with autonomic nervous system activity, a quantitative, computational, and theoretical model of the underlying phenomenon is still lacking. To date, no significant attempts have been made to provide a quantitative explanation of how neurochemical-induced changes in perception impact the spatial mapping of the visual field from physical to perceptual space. Therefore, there remains a unique need to develop such a model, as it could provide insight into the underlying mechanisms and help to further our understanding of the complexities of human visual perception in normality and disease condition.

Several experimental studies have measured the perceptual alterations associated with different sensory modalities under the influence of hyperactivation or hypoactivation agents (Fischer et al., 1969c; Hill et al., 1969; Wittmann et al., 2007). Thus, the hyperactivation and

hypoactivation states alter the neurochemical milieu across the brain and impact the perception associated with the various sensory modalities.

In this study, we focused specifically on the visual system and examined how hyperactivation and hypoactivation situations induced by neuromodulating agents can alter visual spatial perception. To the best of our knowledge, this study presents the first novel quantitative neurophysiological analysis and empirically validated computational model of perceptual alterations and distortions, with respect to the dynamics of hyperactivation and hypoactivation inducing agents in brain tissue. To achieve this, we formulated the kinetics-based action of the neuromodulating biochemicals and developed a geometrical model to describe and understand the corresponding changes in visual spatial perception. We confirmed and validated our computational formulation by analyzing findings from behavioral studies where the subjects were assessed to estimate visuospatial perceptual alteration and distortion under the action of both hyperactivation and hypoactivation-inducing agents. Furthermore, we explored the neuronal basis that can manifest as alterations in visual-spatial perception by modeling a drug action on a computational formulation of the neural grid cell network. Additionally, we used neuroimaging procedure of MRI tractography to identify the neural tracts that may be part of the human brain network responsible for visual-spatial perception.

2.2 Formulation of the Quantitative Framework

2.2.1 The Geometry of Perceived visual space:

The visual system senses optical information about the external physical world and conveys it to the brain through neural signals. The brain interprets this information and constructs a perceptual map of the external world, also known as the visual space. Visual space is a notion defined by the brain to encode the dynamic relationships among the events/objects in the physical visual field, and visual space is the subjective counterpart of physical space.

The external physical world seems euclidean to us, similar to how the geometrical relationships between objects are defined in the cartesian coordinate system. However, it is consistently shown by various studies that the geometry of the visual space has non-euclidean nature (Luneburg, 1947; Indow, 1979; Fernandez and Farell, 2009; Koenderink et al., 2016). Since the activation of the autonomic nervous system elicits the modulation of visual perception (Fischer et al., 1969a, 1969b, 1970; Hill et al., 1969; Fischer, 1971; Hill and Fischer, 1971a), it can be taken that the visual space will remain non-euclidean under the hyper or hypoactivation state. Therefore, hypoactivation and hyperactivation induced alterations in visual perception can be represented by variations in the non-euclidean geometry of the visual space.

We will now explore the mathematical formulation that can represent the geometry of the visual space. The distance (ds) between two infinitesimal closed points whose cartesian coordinates are (x_1, y_1) and (x_1+dx, y_1+dy) on a two-dimensional flat or euclidean space can be calculated using the Pythagoras theorem, as shown in Equation (2.1).

$$ds^2 = dx^2 + dy^2 \tag{2.1}$$

Rewriting Equation (2.1) in matrix form:

$$ds^2 = [dx \quad dy] * \begin{bmatrix} 1 & 0 \\ 0 & 1 \end{bmatrix} * \begin{bmatrix} dx \\ dy \end{bmatrix}$$

$$ds^2 = [dx \quad dy] * g * \begin{bmatrix} dx \\ dy \end{bmatrix} \tag{2.2}$$

However, if two points are located on the curved or non-euclidean space, the Pythagoras theorem does not hold. The distance (ds) between two infinitesimal points can be calculated for the non-euclidean spaces using Equation (2.3).

$$ds^2 = \alpha.dx^2 + \beta.dy^2 + \theta.dxdy + \Phi.dydx \tag{2.3}$$

Rewriting Equation (2.3) in matrix form (* denotes the matrix multiplication):

$$ds^2 = [dx \quad dy] * \begin{bmatrix} \alpha & \Phi \\ \theta & \beta \end{bmatrix} * \begin{bmatrix} dx \\ dy \end{bmatrix}$$

$$ds^2 = [dx \quad dy] * g * \begin{bmatrix} dx \\ dy \end{bmatrix} \tag{2.4}$$

A comparison of Equations (2.2) and (2.4) shows the difference between the non-euclidean and Euclidean spaces. In Euclidean space, the diagonal components of matrix g are unity, and other components are zero. While in the non-euclidean space, the components of the matrix g can be arbitrary, depending upon the underlying geometry. The standard mathematical term for the matrix g is the metric tensor, as depicted in Figure 2.1. The metric tensor (g) in Equation (2.4) is generalizable to the n-dimensional space. In addition to defining the way to measure distances, the metric tensor also expresses the geometrical characteristics of the arbitrary space. Therefore, we will use the metric tensor to indicate the underlying

geometrical variations of the visual space due to the modulation of the visual perception. We illustrated a representative perceived geometry of the physical visual field in Figure 2.2.

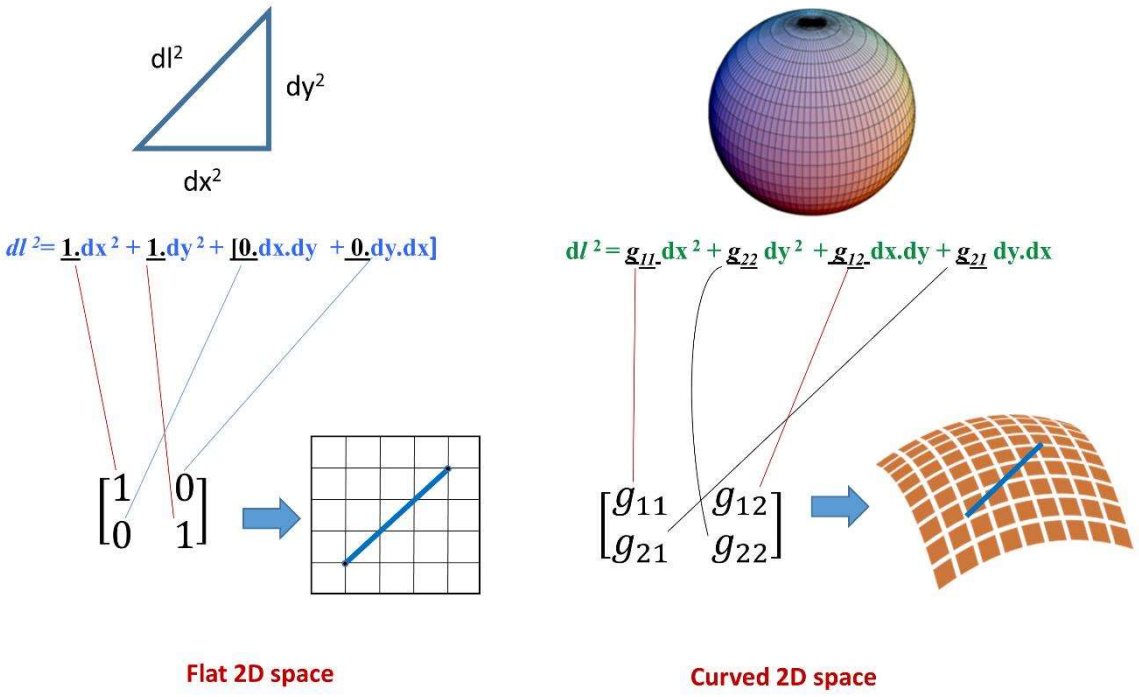

Figure 2.1. Conceptual illustration of the metric tensor for prototypical representative flat two-diemensional space and curved two-dimensinal surface.

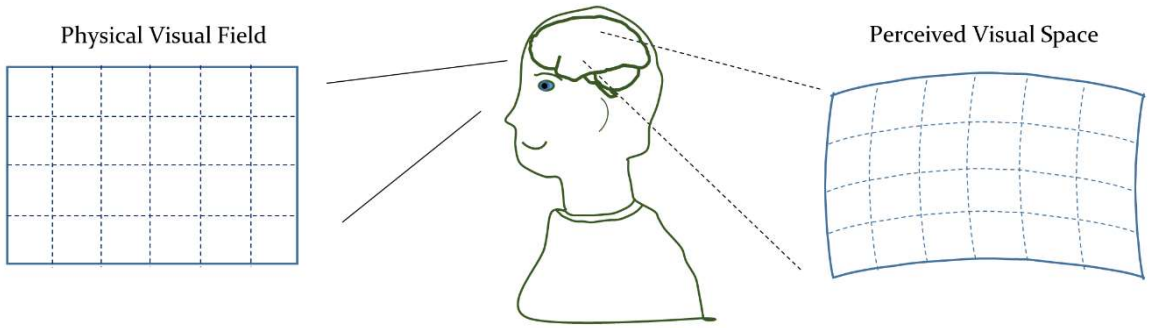

Figure 2.2. Conceptual illustration of the physical space and perceived visual space under the influence of the drug-induced activation of the autonomic nervous system.

As the pharmacological agent is administered, its concentration will gradually increase in the brain's extracellular space after crossing the blood-brain barrier (Pardridge, 2012; Daneman and Prat, 2015), reach a peak, and then decline as the agent is metabolized and excreted via the kidney (Anders, 1980). Since the metric tensor of the perceived visual space (without any pharmacologically-induced nervous system activation) may vary individually due to existing internal and external factors, we will consider the changes in the metric tensor components to quantify the effect of the nervous system activation on visual perception. Several experimental investigations have suggested that visual space may be isotropic (Yartsev and Ulanovsky, 2013; Kim et al., 2017; Kim and Maguire, 2018). Thus, off-diagonal components of the metric tensor may not change significantly due to the alterations of the visual perception, and only diagonal components should be sufficient to capture the dynamic modulatory influence of nervous system activation on visual perception.

Furthermore, the type of nervous system activation affects visual perception oppositely (Fischer, 1971), which can be taken as the opposite changes in the metric tensor components. To paraphrase, hyperactivation can increase the value of the metric tensor components, while hypoactivation can decrease the value of the metric tensor components. An individual's pharmacological tolerance or sensitivity can affect the amount of the drug needed to induce the perceptual alterations, personalised weber constant (P) represent this sensitivity. The lower value of the weber constant indicates that less drug is required to elicit perceptual alterations, i.e., the person has higher sensitivity to the agent.

Hence, we may write the change in the metric tensor in spherical coordinates (r , θ, Φ) as follows in Equation 2.5:

$$\triangle g = \begin{bmatrix} \frac{\mu M g_{rr}^{max}}{P} & 0 & 0 \\ 0 & r^2 \frac{\mu M g_{\theta\theta}^{max}}{P} & 0 \\ 0 & 0 & r^2 \cos\theta \frac{\mu M g_{\Phi\Phi}^{max}}{P} \end{bmatrix} \quad (2.5)$$

where

μ = arousal coefficient

(μ = 1 for hyper-activation and μ = -1 for hypo-activation inducing drugs)

P = Personalized Weber constant

g_{rr}^{max} , $g_{\theta\theta}^{max}$, $g_{\Phi\Phi}^{max}$= Maximum possible deviation in metric tensor (g) components at r=1 and θ=0 (during the peak perceptual effect.)

The metric tensor can also be calculated in any other coordinate system (Oeijord, 2005). In Equation 2.5, M is a modulation index representing the modulatory effect of drug molecules on the visual perception process. The numerical value of the modulation index (M) varies between 0 (no drug condition, $\triangle g$ =0) and 1 (peak perceptual deviation, $\triangle g_{diagonal}$ = g_{rr}^{max} , $g_{\theta\theta}^{max}$, $g_{\Phi\Phi}^{max}$ at r=1 and θ=0). The arousal coefficient (μ) denotes the type of nervous system activation, μ=1 for hyperactivation and μ= -1 for hypoactivation. Note that, in this model, the parameter M can be taken out of the metric in Equation 2.5 as a multiplicating factor. Hence, change in the metric as a response to the drug manifests as a diffeomorphic distortion induced by the parameter M. The change in the parameter M results due to the drug action, as will be shown subsequently.

2.2.2 Parameter for Representing the Alterations:

After diffusing into the extracellular space of the brain, the drug affects neuronal activities by affecting the neurochemical processes, and the subjects start to perceive changes in visual spatial perception, which is evident from the observations of the experimental studies (Fischer et al., 1969c, 1969a, 1969b, 1970; Hill et al., 1969; Fischer, 1971; Hill and Fischer, 1971a). However, experimental studies could measure only perceptual properties/experiences, such as the handwriting area (Fischer et al., 1969c), which is a manifestation of the modulated geometry of the visual space. Since drug-tissue interaction in the brain is a chemical process, corresponding perceptual variations should correlate with the dynamics of this process. The pathways and mechanism of action of drug molecules vary and act differently in the brain depending on the drug's chemical structure (van Rossum, 2011). However, irrespective of the drug's chemical structure, drug molecules can affect the firing characteristics of the neurons and modulate the inter-neuronal signaling in the neuronal networks responsible for perceptual functions, albeit differently.

Let us assume that the n molecules of the drugs can modulate the activity of one neuron, since this is a chemical process, Equations 2.7a and 2.7b below represent this process in terms of a chemical reaction. The terms k_f and k_r are the forward and reverse reaction rate constants, respectively. To paraphrase, a neuron has multiple binding sites for the drug molecules, out of which binding of drug molecules at n sites will cause the alteration in the activity of that neuron.

The forward reaction is:

$$\text{neuron} + n\ (\text{drug molecule}) \xrightarrow{k_f} \text{neuron-drug molecule complex} \tag{2.6a}$$

The reverse reaction is:

$$\text{neuron-drug molecule complex} \xrightarrow{k_r} \text{neuron} + n\ (\text{drug molecule}) \tag{2.6b}$$

Let us denote neuron by **N**, drug molecule by **C**, and neuron-drug molecule complex by **NC**. Here, **N** is a neuron whose activity is unaffected, while **NC** is a neuron whose activity is modulated by the drug action. Then equations 2.6a and 2.6b become as follows:

$$\mathbf{N} + \text{n}\ (\mathbf{C}) \xrightarrow{k_f} \mathbf{NC} \tag{2.7a}$$

$$\mathbf{NC} \xrightarrow{k_r} \mathbf{N} + \text{n}\ (\mathbf{C}) \tag{2.7b}$$

Using mass-action law:

$$\frac{d[\mathrm{C}]}{dt} = -k_f.[N].[\mathrm{C}]^n + k_r.[NC] \tag{2.8a}$$

$$\frac{d[N]}{dt} = -k_f.[N].[\mathrm{C}]^n + k_r.[NC] \tag{2.8b}$$

$$\frac{d[NC]}{dt} = k_f.[N].[\mathrm{C}]^n - k_r.[NC] \tag{2.8c}$$

At equilibrium condition:

$$\frac{\mathrm{d}[\mathrm{C}]}{\mathrm{dt}} = 0$$

Then, from Equation 2.8a:

$$k_f.[N].[\mathrm{C}]^n = k_r.[NC]$$

$$[NC] = \left(\frac{k_f}{k_r}\right).[N].[\mathrm{C}]^n \tag{2.9}$$

Adding [N] on both sides of Equation 2.9:

$$[NC] + [N] = \left(\frac{k_f}{k_r}\right).[N].[C]^n + [N] \quad (2.10)$$

Dividing Equation 2.9 by Equation 2.10 yields the following:

$$\frac{[NC]}{[NC]+[N]} = \frac{\left(\frac{k_f}{k_r}\right).[C]^n}{\left(\frac{k_f}{k_r}\right).[C]^n + 1}$$

$$\frac{[NC]}{[NC]+[N]} = \frac{1}{1 + \frac{k_r}{k_f[C]^n}} \quad (2.11)$$

Let $\frac{k_r}{k_f} = k^n$, then Equation 2.11 becomes:

$$\frac{[NC]}{[NC]+[N]} = \frac{1}{1 + \frac{k^n}{[C]^n}} \quad (2.12)$$

Now, we define the modulation index (M) as the ratio of the "number of neurons whose activity is influenced by the drug-induced nervous system activation" and "the maximum number of the neurons available for the drug action" (i.e., M can be described as the relative activation parameter of neurons, namely the fraction of the neurons that are activated). We can express the modulation index (M) in mathematical form, as follows:

$$M = \frac{[NC]}{[NC]+[N]} \quad (2.13)$$

Thereby, from Equations 2.12 and 2.13:

$$M = \frac{1}{1 + \left(\frac{k}{C}\right)^n} \quad (2.14)$$

Let us put M=1/2 into Equation 2.14, then:

$$\left(\frac{\mathrm{k}}{C}\right)^{n} = 1$$

Since n ≠ 0, therefore k = C. Hence the numerical value of k equals the drug concentration required to produce M=0.5 or 50 percent modulation level compared to the maximum modulation of the visual spatial perception.

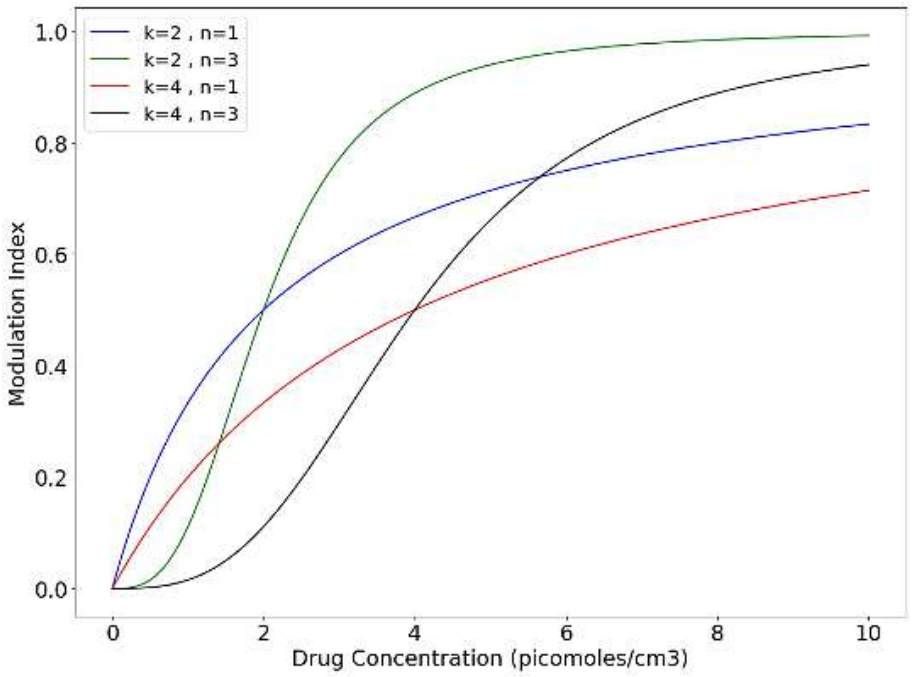

Figure 2.3. Variation in modulation index (M) as drug concentration (C) changes, with different values of the n (Hill coefficient) and k (Half-effective drug concentration) for illustrative purposes.

Equation 2.14 is similar to the Hill equation, which is often used in biochemistry (Frank, 2013). Indeed, the occurrence of the Hill equation in our approach is not unexpected as drug-induced modulation of the visual-spatial perception is also a neurochemical process at the molecular level. Comparing the standard Hill equation and Equation 2.14 concludes that n

is a Hill coefficient. The modulation index (M) is a function of the drug concentration (C), Hill coefficient (n), and k (half effective drug concentration). The value of M = 1 denotes the peak perceptual response of the drug action, while M=0 denotes the normal condition. The Hill coefficient (n) determines the rate of change of modulation index with changes in drug concentration, as depicted in Figure 2.3. In the following subsection, we will formulate a mathematical dynamical model of the drug dynamics after ingesting a particular amount.

2.2.3 Dynamics of the Neuromodulating Agents in the Brain:

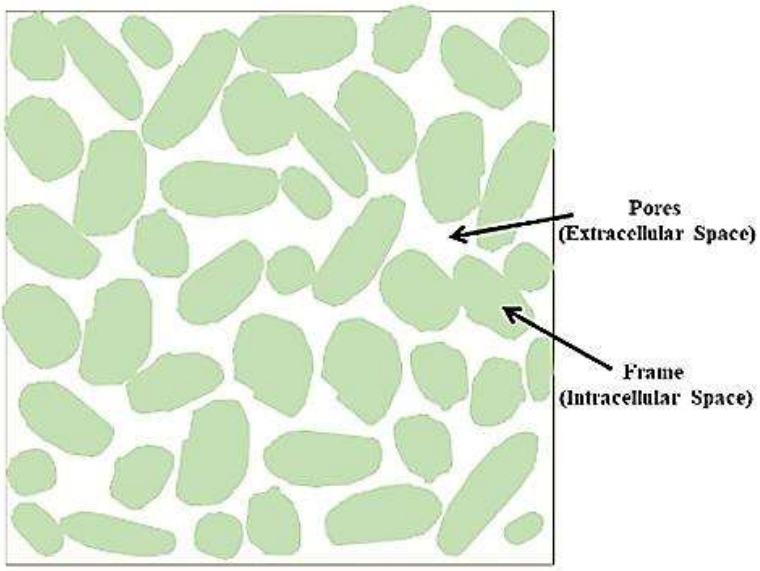

Figure 2.4. Simplified two-dimensional cross-sectional representation of the brain as a porous medium.

Now, we will formulate a quantitative model of drug dynamics in the brain tissue. Drugs can induce either neurophysiological hyperactivation or hypoactivation. After the drug ingestion, the drugs cross the blood-brain barrier, whence the drug molecules diffuse into the extracellular space of the brain tissue (Pardridge, 2012; Daneman and Prat, 2015). Brain parenchyma is not a continuous space; therefore, it is not a free but rather a restricted diffusion.

Therefore we are considering the brain as a porous medium (Gitis and Rothenberg, 2020) for the diffusion of drug molecules. The solid part of the porous medium is called the frame, and gapes between them as pores (Gitis and Rothenberg, 2020). Applying the concepts of the porous media in the case of the brain yield that the intracellular and extracellular spaces (Sun and Sun, 2021) are the frame and pores (Gitis and Rothenberg, 2020), respectively, as shown in Figure 2.4. The intracellular space consists of the internal portion of the neuronal cells, while the extracellular space is the empty portion between neuronal cells filled with interstitial fluid (Sun and Sun, 2021).

Due to the porous structure of the diffusion space, the effective diffusivity of the drug molecules decreases by the factor of the square of the tortuosity (Lehner, 1979), where tortuosity (TS) is the ratio of the actual distance traced by the drug molecules and straight line distance (i.e. displacement). Using Fick's second law (Macdonald, 1977) to represent the drug diffusion in the porous medium (Equation 2.15):

$$\frac{\delta C}{\delta t}_{diffuson} = \frac{D}{TS^2}\left(\frac{\partial^2 C}{\partial x^2} + \frac{\partial^2 C}{\partial y^2} + \frac{\partial^2 C}{\partial z^2}\right) \tag{2.15}$$

where:

D = Diffusivity of the drug molecules in the extracellular space (cm^2 per second)

TS = Tortuosity

C = Drug concentration (moles per cm^3)

x, y, z : axes of the three-dimensional cartesian coordinate system.

The porosity reduces the accessible volume available to the drug molecules by the factor of the volume fraction (α - the ratio of extracellular space volume and total volume)

(Nicholson et al., 1979; Nicholson and Phillips, 1981). Next, drug molecules' movement from the blood to the extracellular space through the blood-brain barrier depends on the transfer coefficient for the drug molecules from brain tissue to the blood (k_{po}) and instantaneous drug concentration in the blood (C_a) (Patlak and Fenstermacher, 1975). Another transfer coefficient for the drug molecules from the blood to the brain tissue (k_{pi}) and instantaneous drug concentration in the brain (C) determines the dynamics of drug molecules crossing from the brain's extracellular space to the vascular supply to the brain (blood) (Patlak and Fenstermacher, 1975).

Hence, we can represent the phenomenons mentioned above in mathematical form as follows (Equation 2.16):

$$\frac{\delta C}{\delta t}_{movement} = \frac{1}{\alpha}(k_{po}C_a - k_{pi}C) \tag{2.16}$$

For our analysis, we are discounting the bulk flow of the drug molecules, as diffusion is the dominant process involved in the dynamics of the drug molecules (Ohata and Marmarou, 1992). Furthermore, we can take that the drug molecules are not diffusing from the extracellular space to the intracellular space. Using Equations 2.15 and 2.16, we can now formulate a differential equation (Equation 2.17) to represent drug dynamics in the brain where drug concentration (C) varies with time (t) and spatial location (x,y,z).

$$\frac{\partial C}{\partial t} = \frac{D}{TS^2}\left(\frac{\partial^2 C}{\partial x^2} + \frac{\partial^2 C}{\partial y^2} + \frac{\partial^2 C}{\partial z^2}\right) - \frac{(k_{pi}C - k_{po}C_a)}{\alpha} \tag{2.17}$$

where:

C [= C(x,y,x,t)] =Drug concentration in the extracellular space (moles per cm^3)

k_{pi} = Transfer coefficient for the drug molecules from brain tissue to the blood (per minute)

k_{po} = Transfer coefficient for the drug molecules from the blood to the brain tissue (ml per gram of tissue per minute)

C_a = Concentration of the drug in the plasma (moles per ml)

α = Volume fraction of the extracellular space with respect to the total volume.

2.2.4 Neural Correlates

2.2.4.1 Multi-Modal Sensory Perception System

In the previous sections, we have represented hyperactivation and hypoactivation induced alterations in the visual-spatial perception as a metric tensor of the perceived visual space whose components vary depending upon the type of the drug and the amount of the dose, as evident from Equation 2.5. The metric tensor defines the mathematical basis to compute the distances on the geometry of the perceived visual space. As per our formulation, the metric tensor components alter due to the modulatory action of the drug molecules.

Now we demarcate the neuronal procedures that may be utilized in the brain for the metric representation of the perceptual space related to the different perceptual modalities, such as visual space, auditory space, olfactory space, and sensorimotor representational space. Neuronal recordings from the entorhinal cortex of the freely moving rats led to finding the spatially modulated receptive field of the grid cells (Hafting et al., 2005). Grid cells in the entorhinal cortex encode position in the navigation space and correspond to the metric component of the navigational space (Moser et al., 2008; Dang et al., 2021). Grid cells exist in

the entorhinal cortex of bats, monkeys, and humans (Yartsev et al., 2011; Killian et al., 2012a; Jacobs et al., 2013). Apart from the entorhinal cortex, grid cells-like neural representations exist while navigating in the olfactory space, auditory space, and sensorimotor space, indicating a general nature of the grid cells to represent metric cognitive maps associated with different types of sensory modalities (Constantinescu et al., 2016; Horner et al., 2016; Aronov et al., 2017; Bao et al., 2019; Long and Zhang, 2021). Initially proposed by Tolman, the brain represents and organizes the information or concepts and extracts the relationships between them from the cognitive map (Tolman, 1948).

As we have delineated above, the grid cell-like neuronal representation is associated with various perceptual modalities. Similarly, in the case of visual space, activation of the grid cell in the entorhinal cortex is observed during (i) the head-fixed monkeys gazing at different images (Killian et al., 2012a) and (ii) humans fixating on randomly appearing targets at different locations in the virtual visual environment (Nau et al., 2018). However, grid cells can exist outside the entorhinal cortex, e.g., in the primary somatosensory cortex. Grid cell activity has been experimentally recorded in the primary somatosensory cortex while rats explored the given arena for the food pellets (Long and Zhang, 2021). In another experiment, the grid cell activity in the medial entorhinal cortex was recorded in rats collecting randomly thrown food pellets in an enclosure (Hafting et al., 2005). In these two experiments, the rats were doing the same task – foraging for the food pellets. But, grid cells were observed in the different brain regions (entorhinal cortex and primary somatosensory cortex). Therefore, we can infer that multiple simultaneous grid cell-based neural maps can exist during a particular task.

During navigation, grid cells in the entorhinal cortex can maintain their firing map independent of the environmental clues. However, path integration in grid cells integrates

direction and speed information with firing positions (McNaughton et al., 2006). Considering the rats foraging for the food task, we can formulate that (i) the somatosensory system provides the necessary information for path integration to the grid cells in the entorhinal cortex and (ii) the somatosensory cortex organizes this path integration information in grid cells-like representation, thus constituting a local spatial map.

2.2.4.2 Mapping of Visual Space by Grid Cells based Motif:

We can now adapt our analysis to visual-spatial perception. Here, we consider two investigations: (i) the experimental observation of the grid cells in the entorhinal cortex during a visual task (Killian et al., 2012a), and (ii) another experimental observation of the encoding of the spatial position in the primary visual cortex (Saleem et al., 2018). Accordingly, we may indicate that the grid cell-like activity should be present in the visual cortex, constituting a local visuospatial map. In the case of the visual system, grid cell like mapping is experimentally recorded in the area V2 of the visual cortex (Long et al., 2021). Indeed, we can posit this mapping because of the resemblance of functional cell population in the medial entorhinal cortex with (i) area V2 and with (ii) broader association cortices in the cerebral hemispheres (Moser et al., 2014).

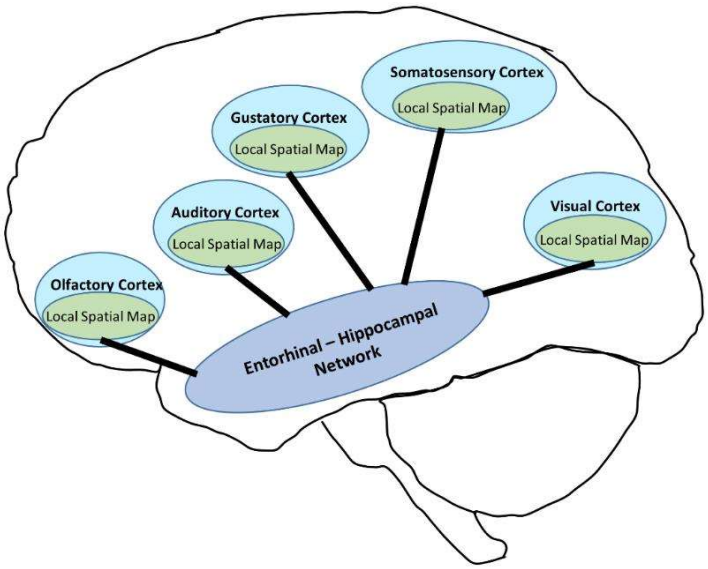

Figure 2.5 Conceptual interconnection complex between the Entorhinal-Hippocampal network and the various local spatial maps at different sensory cortices (e.g., visual, auditory, olfactory, or somatosensory cortices), each sensory cortex is responsible for the metric-oriented representation of the perceived sensory space in that cortex.

Likewise, since the entorhinal plan can be the motif of broader cerebral cortical regions (Hawkins et al., 2019; Chen et al., 2022), then it can be construed that the local maps encoded by grid cells may be present in the other sensory modalities, and these maps may be linked to the entorhinal-hippocampal network for integrating sensory information with the prior information (memory). We represented our conceptual model in Figure 2.5, involving the different sensory modalities. Furthermore, the grid cells are present in the orbitofrontal cortex, posterior cingulate cortex, ventromedial prefrontal cortex, and retrosplenial cortex (Constantinescu et al., 2016; Aronov et al., 2017). Hence, we can implicate that the grid cell like representation also encodes higher-level cognitive conceptual maps in various cortical systems in addition to the sensory-perceptual maps and these grid cells are linked to the hippocampal-entorhinal cortex network.

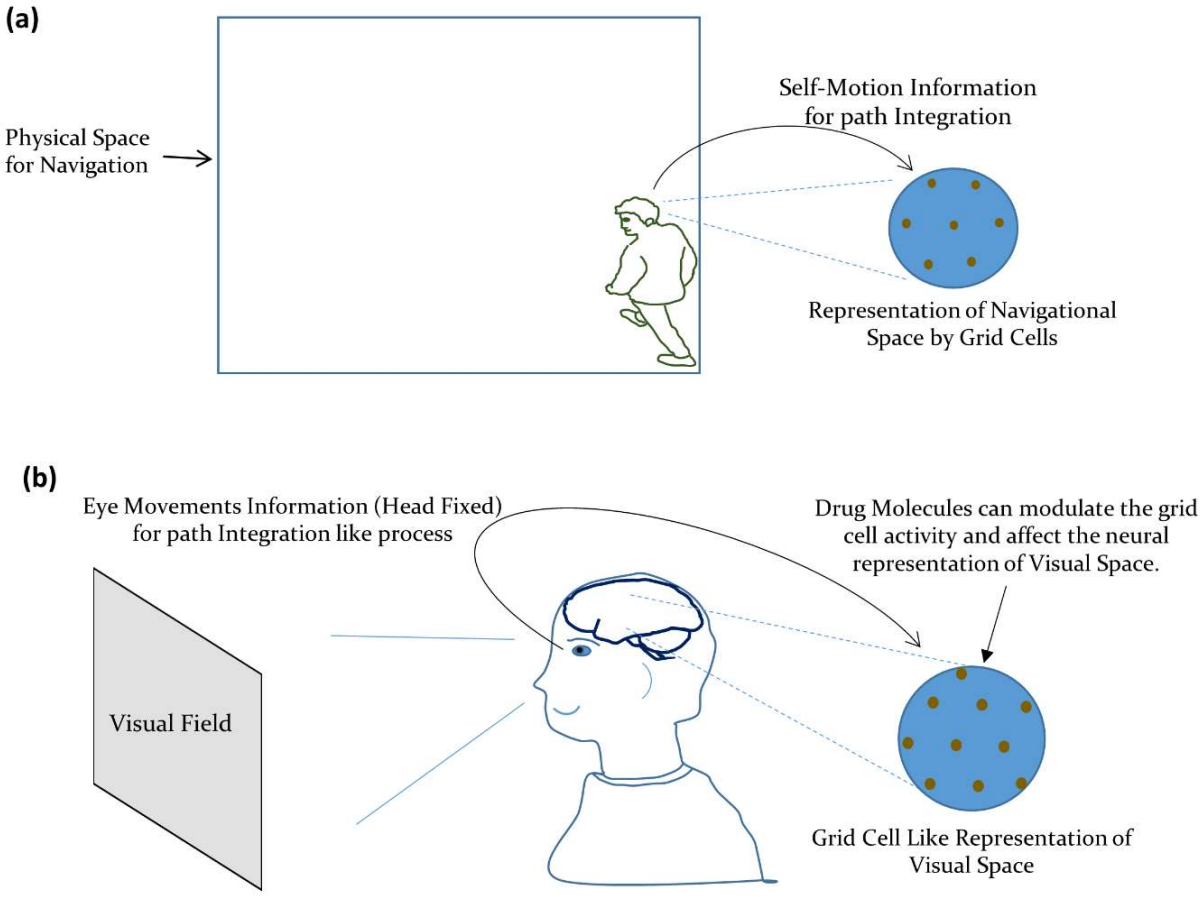

Figure 2.6. (a) Grid cells encode the navigational space by integrating the self-motion information for path integration. **(b)** Our formulation of the metric representation of the visual space by grid cells by integrating the information about the eye movements for path integration like process.

When applied to a specific sensory modality as the visual system, we can now indicate that this integrated network of the 'local spatial map in the visual cortex' and the 'entorhinal-hippocampal network' may be taken to represent the geometry of the perceived visual space. Thus, the modulation of the perceived visual space due to drug-induced activation of the autonomic nervous system can be taken as due to the alteration in the activity of: (i) the aforesaid integrated network of the entorhinal-hippocampal system and (ii) local spatial map

at the visual cortex. This modulation may manifest as the change in the metric tensor components as a consequence of the modification in the grid cell representation of visual space at the neuronal level, under the effect of the drug. In the case of the navigational space, the grid cell encodes the external spatial location by integrating the self-motion information (Figure 2.6(a)) (Etienne et al., 1996; Jeffery et al., 1997; McNaughton et al., 2006). However, in the case of the visual space, the eye movements (with the head fixed) can be taken as the primary information required for path integration like process in the grid cells. This is supported by the experimental observations where the grid cell representation emerged under the eye moving to explore the visual field (Killian et al., 2012a; Nau et al., 2018). We have depicted our formulation in figure 2.6(b).

2.2.4.3 Neuro-computational Model of Drug-Induced Perceptual Alterations

Firing patterns of different grid cells encode the necessary spatial information, and the firing field of a grid cell is characterized by three properties: grid scale, grid orientation, and grid spatial phase (Anton et al., 1970; Hafting et al., 2005; Aronov et al., 2017). Since a single grid cell has a periodic spatial field, it cannot encode a unique position. Nevertheless, the network of the grid cells (having different firing field characteristics and organized in different modules (Stensola et al., 2012)) can encode the unique positions. Thereby, we can formulate that the grid cell networks encode perceived space, consequently playing an essential role in the metric representation of the perceptual space of an individual.

It has been consistently shown that continuous attractor networks can model grid cell networks and firing patterns of the grid cells (Fuhs and Touretzky, 2006; McNaughton et al., 2006; Burak and Fiete, 2009a; Couey et al., 2013). A continuous attractor network has a

continuous set of states toward which the network evolve (Amit, 1989). The toroidal connectivity between the nodes in the continuous attractor network implements the periodic boundary for path integration (Samsonovich and McNaughton, 1997). Recently, the 3-D visualization of the experimentally obtained grid cell activity yielded a torus geometry where points on the torus correspond to the position in the physical space and thus validated the toroidal topology used in the theoretical models of the grid cell networks (Gardner et al., 2022; Hermansen et al., 2022).

Let us consider a neural network with continuous attractor dynamics that participate in mapping the visual space with connections between nodes in the neural network to form a toroidal topology. Based on the experimental observations (Killian et al., 2012b; Nau et al., 2018), we can take that eyeball movement (with head-fixed) provide information about the relative position in the external visual field to the neural network (similar to the self-motion information (path integration (Etienne and Jeffery, 2004)) in the case of the navigation space (McNaughton et al., 2006)). Now we are constructing a neuronal network model inspired by the computational models of grid cells (McNaughton et al., 2006; Guanella et al., 2007a; Burak and Fiete, 2009b). The activity of a node P_j at time t+Δt is as follows (Equation 2.18), where N is the total number of nodes and λ is stabilization strength, where the nodes of the neural network forming a torus topology (Guanella et al., 2007b).

$$P_j(t+\Delta t) = (1-\lambda)\sum_{i=1}^{i=N} P_i(t)\, W_{ij}(t) + \lambda\left(\frac{\sum_{i=1}^{i=N} P_i(t)\, W_{ij}(t)}{\sum_{i=1}^{i=N} P_i(t)}\right) \qquad 2.18$$

Equation 2.18 shows that the W_{ij} is the connection weight between node P_i and P_j. As shown by Equation 2.19 below, the weight (W_{ij}) follows the gaussian function, which depends

on the toroidal distance ($\|...\|_{toroidal}$) between the node P_i and P_j (McNaughton et al., 2006) , and eyeball speed vector ($E(t) = \{E_\theta, E_\Phi\}$ where θ and Φ are angular coordinates of the fixation point). T determines the ratio of the excitatory and inhibitory connections, and I affects the interaction strength between the node P_i and P_j while Z_i and Z_j are the coordinates of the node P_i and P_j on the torus.

$$W_{ij}(t) = I\, e^{-\left(\frac{\left\| z_i - z_j + E(t)\right\|^2_{toroidal}}{s^2}\right)} - T \qquad 2.19$$

The equations mentioned above (2.18 and 2.19) are reformatted from Equations 1, 2, and 14 of Guenella et al., 2007, specific to our case. Now let us analyze the above-mentioned neural network model of the grid cell network under different conditions:

Case-1: Normal Condition (without any autonomic nervous system activation):

(i) *Eyes fixating on a target in the visual field:* In this condition, the eyeball speed vector will be zero (E(t)=0), and thus W_{ij} in this situation will be as follows (Equation 2.20):

$$W_{ij}(t) = I\, e^{-\left(\frac{\left\| z_i - z_j\right\|^2_{toroidal}}{s^2}\right)} - T \qquad 2.20$$

In this case, the weights (W) will be constant with time. Therefore few nodes (grid cells) in the network will constantly be active (independent of time) depending upon the firing characteristics (grid scale, grid orientation, grid phase), thereby encoding the fixation point in the visual space.

(ii) *Eyeball moving to scan the visual field:* In this condition, the eyeballs move with time; therefore, the eyeball speed vector will be non-zero ($E(t) \neq 0$). The weight (W) will change with time (Equation 2.19). Because of the temporal variation in the weights among the nodes,

the activity of the nodes will change with time. Since grid cells have spatially periodic firing patterns, the several nodes will show periodic activation if the eyeballs move beyond the spatial period of that particular node.

Case-2: Under drug-induced activation: After the drug ingestion, the drug molecules can modulate the population activity of the grid cell network by binding with the receptors on the grid cell or indirectly through another pathway, as discussed in an earlier section. There transpires to be experimental corroboration of drug-induced alteration of spatial mapping due to modulation of neuronal coding. For instance, experimental electrophysiological studies show that due to the modulatory effect of the excitatory-inhibitory interactions, the synaptic weights of the grid cell network could change (Shipston-Sharman et al., 2016). Another experimental corroboration comes from an empirical investigation (Bonnevie et al., 2013) which demonstrates that there are alterations in the synaptic weights due to the change in grid cell network activity induced by pharmacological agents that produce synaptic modulation, such as muscimol (a GABA agonist and hypoactivation-inducing agent).

Therefore, we can assume that the drug molecules modulate the weight between the nodes of the neural network. However, the modulation of the weights will not be uniform across neural network because the concentration of drug molecules will not be the same at every spatial coordinate in the brain, as indicated by Equation 2.17. Instead, the synaptic weight modulation shall depend on the local concentration of the drug molecules around the grid cell (node). Hence, to quantify the modulatory effect of the drug molecules, the physical location of the neurons and the drug concentration at that location will be require.

In our model, drug action modulates the weights (W) by affecting the interaction (I) between the nodes. We can express the change in the interaction as node *i* act as input to the

node *j* ($\triangle I_{ij}$) as a function (f) of the drug concentration (C) in the infinitesimal volume around node *i.*

Therefore, in mathematical terms, we can write that:

$$W_{ij}(t) = (I + \triangle I_{ij}(t))\, e^{-\left(\frac{\left\| z_i - z_j + E(t) \right\|^2_{toroidal}}{s^2}\right)} - T \qquad 2.21$$

where:

$$\triangle I_{ij}(t) = b * f\left(\frac{\int_{x_i}^{x_i+\triangle x}\int_{y_i}^{y_i+\triangle y}\int_{z_i}^{z_i+\triangle z} C(x,y,z,t)\, dxdydz}{\triangle x \triangle y \triangle z}\right) \qquad 2.22$$

In Equation 2.22, $\triangle x \triangle y \triangle z$ is an infinitesimal volume around the node (grid cell), (x_i, y_i, z_i) are the physical coordinates of the node P_i in the brain, and **b** is a scaling factor. Equation 2.22 also highlights that the "$\triangle I_{ij}$" is a function of the spatial coordinates (x,y,z) and time (t). Further, considering that the neural network is located within a microvolume where the drug distribution can be considered spatially uniform, then "$\triangle I_{ij}$**"** will depend mainly on time (t).

Now let us analyze the above-mentioned neural network model of the grid cell network under the following conditions:

(i) *Eyes fixating on a target in the visual field:* In this condition, the eyeball speed vector will be zero (E(t)=0), and W_{ij} in this situation will be as follows (see Equation 2.19):

$$W_{ij}(t) = (I + \triangle I_{ij}(t))\, e^{-\left(\frac{\left\| z_i - z_j \right\|^2_{toroidal}}{s^2}\right)} - T \qquad 2.23$$

As shown by Equation 2.23, the weights (W) will change with time, depending on the drug dynamics. Therefore some nodes (grid cells) in the network will be active at a particular moment, and then another set of nodes will become active as soon as the weights (W) will alter due to a change in local drug concentration. Nevertheless, the nodes may not show periodic spatial activation since the eyeballs are not moving in the visual field. However, the neuronal coding of the visual space will get modulated due to the activation of a different set of nodes.

(ii) Eyeball moving to scan the visual field: In this condition, the eyeballs move with time; therefore, the eyeball speed vector will be non-zero ($E(t)\neq 0$). The weight (W) will change with time (Equations 2.21 and 2.22) due to eyeball movements and the modulatory action of the drug molecules. Since grid cells have spatially periodic firing patterns, the several nodes will show periodic activation if the eyeballs move beyond the spatial period of that particular node.

However, contrary to the *no-drug* condition, the drug action should cause alterations in the activation pattern of the grid cell (such as grid scale, grid period, or grid phase) to enable the corresponding alteration in the mapping of perceived visual space.

2.3 Experimental Validation of Quantitative Framework

2.3.1 Methodology

2.3.1.1 Dynamics of Psilocybin

We obtained indicative parameters for psilocybin from various experimental studies to solve Equation 2.17. Tortuosity (TS) and volume fraction (α) are the anatomical features and do not depend on the drug being ingested. We found average values for the normal brain, TS = 1.6 and α = 0.2 (Cserr et al., 1991; Lehmenkühler et al., 1993; Perez-Pinzon et al., 1995; Kume-Kick et al., 2002; Zhu et al., 2020). We calculated the diffusion coefficient for the psilocybin in water at normal brain temperature (37^{O} C) using the well-known linear analytic relationship between molecular weight and diffusion coefficient (Evans et al., 2013, 2018). The diffusion coefficient in the extracellular space (ECS) is 40 percent of the value in the water (Patlak and Fenstermacher, 1975; Fenstermacher and Davson, 1982), therefore, the calculated diffusion coefficient of the psilocybin in the ECS is 3.052×10^{-10} meter^2/second.

We calculated (i) brain-to-blood transfer coefficient (K_{pi}) and (ii) blood-to-brain transfer coefficient (K_{po}) for psilocybin, based on experimental observations from other drugs (in the literature, there is an absence of any experimental study which directly measures transfer coefficients for psilocybin). We utilized the brain-to-blood and blood-to-brain transfer coefficient of the Meglumine Iothalamate (molecular weight: 809) (Groothuis et al., 1990), Iopamidol (MW:777) (Ivan Yeung et al., 1992) and alpha-aminoisobutyric acid (molecular weight: 104) (Blasberg et al., 1983) , to calculate K_{pi} and K_{po} of the psilocybin (molecular weight: 284.25) using the linear interpolation technique. After mathematical analysis, we obtained $K_{pi}=16.38\times10^{-3}$ per minute and $K_{po}=1.4\times10^{-3}$ ml/gram of tissue/minute for psilocybin.

Next, we found out the average psilocybin concentration in blood (C_a) by assessing from seven healthy subjects in a different study recently, where the assay was performed using high-performance liquid chromatography after oral ingestion of the psilocybin (Lindenblatt et al., 1998). Thereafter, we applied the finite difference method for the partial differential equation to solve Equation 2.17 with a temporal step size of 0.01 minutes, a spatial step size (three dimensions) of 0.01 centimeters. We approximated the spatial volume as equal to the average brain volume (~1300 cm^3) (Ricard et al., 2010). We wrote a python program and calculated the temporal variation of the psilocybin concentration in the brain for 2000 minutes, i.e., about 33 hours, which is comparatively a long duration, and by that time vast majority of psilocybin had been excreted by the subject. [The corresponding codes are available at: https://github.com/pratik-purohit/modulation-visual-perception]. For computing, we utilized the facility of the National Supercomputing Mission of the Govt. of India (Institutional Param-Shivay Supercomputer facility).

2.3.1.2 Dynamics of Chlorpromazine

We utilized different parameters regarding the chlorpromazine dynamics in the brain from various experimental studies, to solve Equation 2.17. For instance, the average values of tortuosity (TS) and volume fraction (α) for the normal brain are 1.6 and 0.2, respectively. Then, we calculated the diffusion coefficient for chlorpromazine in water at 37^O C using the same method used for psilocybin and arrived at our derivation of D (chlorpromazine in ECS) = 2.9 x 10^{-10} $meter^2$/second. Furthermore, we derived k_{pi}= 16.65 x 10^{-3} ml/gram of tissue/minute and k_{po}=1.43 x 10^{-3} per minute for chlorpromazine using the method explained in earlier section. Next, we availed of the average chlorpromazine concentration in the blood through information

from experimental measurements from the eleven healthy subjects using the extraction radioimmunoassay method after oral ingestion of the 100 mg chlorpromazine (Yeung et al., 1993). Thence, we applied the finite difference method for the partial differential equation to solve Equation 2.17 with a temporal step size of 0.01 minutes, spatial step size (three dimensions) of 0.01 centimeters, and approximated the spatial volume equal to the average brain volume (~1300 cm^3) (Ricard et al., 2010). We constructed a python program and calculated the temporal variation of the chlorpromazine concentration in the brain for 2500 minutes. i.e. about 41 hours, which is a substantial duration, and by that time virtually vast majority of chlorpromazine has been eliminated by the subject. [The corresponding codes are available at: https://github.com/pratik-purohit/modulation-visual-perception].

2.3.1.3 Diffusion MRI Experiment

3 Tesla MRI: The diffusion weighted MRI scans of 30 subjects (cognitive normal) were randomly selected from the Open Access Series of Imaging Studies (OASIS) image bank (LaMontagne et al., 2019). Ethics committee approval was given by the Knight Alzheimer Disease Research Center at Washington University, St. Louis, USA. The diffusion MRI scans were rotated to align with the AC-PC line. The accuracy of b-table orientation was examined by comparing fiber orientations with those of a population-averaged template (Yeh et al., 2018). The tensor metrics were calculated using DWI with b-value lower than 1750 s/mm^2. A deterministic fiber tracking algorithm (Yeh et al., 2013) was used. After preprocessing, we used the following tracking parameters in DSI Studio software (http://dsistudio.labsolver.org) to find the neural tracts: anisotropy threshold was 0.04162, the angular threshold was 70 degrees, the step size was 0.01 mm, and a total of 100000 seeds were placed.

7 Tesla MRI: Scans were acquired on a 7T Siemens MAGNETOM scanner at Maastricht University, Netherlands (Gulban et al., 2019). Approval was given by Ethics Committee of the Faculty for Psychology and Neuroscience at Maastricht University (reference number: ERCPN167_09_05_2016), and informed consent was obtained. Diffusion-weighted MRI images were scanned using multi-band diffusion-weighted spinecho EPI protocol with following parameters: b-values = 1000, 2000 and 3000 s/mm2, FOV = 200 x 200 mm with partial Fourier 6/8, 132 slices , 1.05 mm isotropic voxel size, TR = 7080 ms, TE = 75.6 ms, 66 directions and 11 additional b = 0 volumes for every b-value (Gulban et al., 2019). Susceptibility artifact was estimated using reversed phase-encoding b0 by TOPUP from the Tiny FSL package (http://github.com/frankyeh/TinyFSL), a re-compiled version of FSL TOPUP (FMRIB, Oxford) with multi-thread support. FSL eddy was used to correct for eddy current distortion. After preprocessing the MRI image, we used DSI Studio software (http://dsistudio.labsolver.org) for deterministic tractography using the diffusion tensor imaging technique (Basser et al., 1994). We used Brainnetome Atlas to locate the region of interest (ROI) (Fan et al., 2016). The tracking parameter was fractional anisotropy threshold 0.1784, angular threshold 65 degrees, step size 0.1mm, and 1000000 seeds. We performed this analysis pipeline for one normal subject (Gender: Female, Age: 27 years).

2.3.1.4 Computational Model of a Grid Cell Network

We simulated a neural network-based model of the grid cells, where nodes (grid cells) were arranged on the two-dimensional surface. The total number of nodes were 90 (= 9 x 10). The nodes were arranged on the surface of the torus, as illustrated in Figure 2.7 below, and the distances between nodes were calculated, accordingly. Therefore, the arrangement of the nodes constituted the periodic boundary. The circumference of the minor and major circles of the

torus were 0.5 and 0.61, respectively. Here, one should note that torus topology is defined to assign the weights and connectivity among the nodes (depending on their distances on the toroidal surface). However, the physical positions of the grid cells in the brain may not constitute toroidal topology.

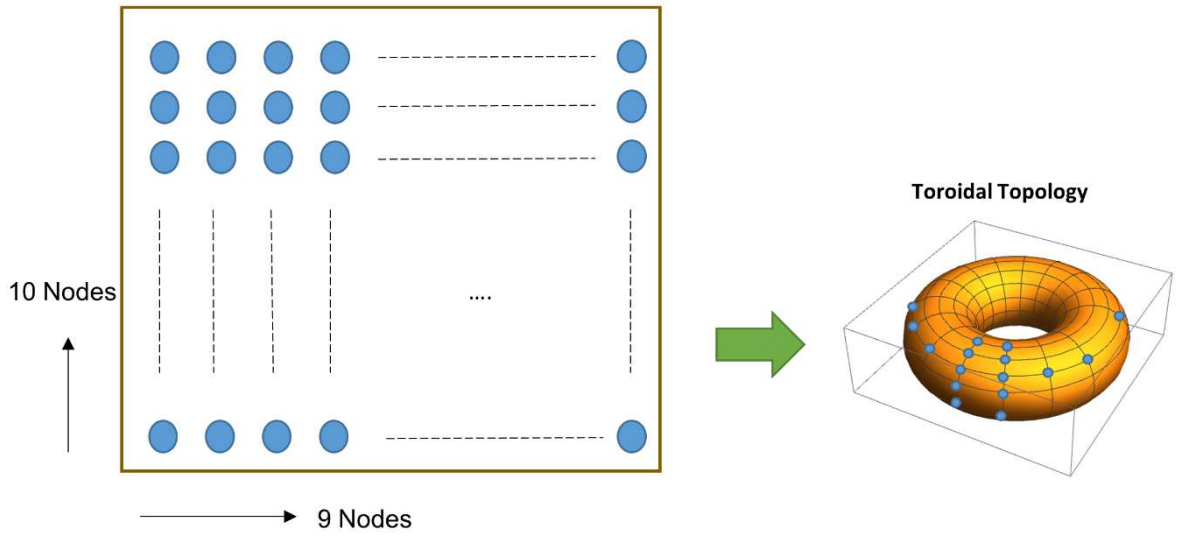

Figure 2.7. The arrangement of the nodes in the neural network model of the grid cells.

We used Equation 2.18 to calculate the activity of nodes at time t+Δt, which depends on the activity of the network at time t and weights (W), using Δt = 0.01 seconds and λ = 0.8. The initial activity of the nodes at time t=0 was randomly distributed between 0 and $\mathbf{1/\sqrt{90}}$ (total number of nodes=90). Equation 2.21 provides the weights between the nodes under the: (i) drug-induced neural activation (ΔI≠0) and (ii) normal condition (no-drug condition, ΔI=0), keeping s=0.24 and T=0.05.

Since there are only 90 grid cells (nodes) in our network, we assumed that the local drug concentration at each node would be almost equal at any instant. Therefore, the weights (W) will be affected equally as the drug concentration changes with time. We evaluated the

effect of the drug molecules on the grid cell activity by calculating the network activity for 4 seconds (time step: 0.01 seconds) for different values of the ΔI (0 to 0.30). We used python programming language to implement the neural network model of the grid cell [the corresponding codes are available at: https://github.com/pratik-purohit/modulation-visual-perception]. We observed the network activity under the following situations, separately for under the *no-drug* condition and under *the drug-induced activation* condition:

a) Eye Fixation: E(t)=0.
b) Eye moving in the visual field:
    - Eyeballs scanning the visual field with constant movement (E(t)=constant)
    - Eyeballs scanning the visual field randomly (E(t)=random)

2.3.1.5 Measurement of Visual Space Under Hyper-Activation

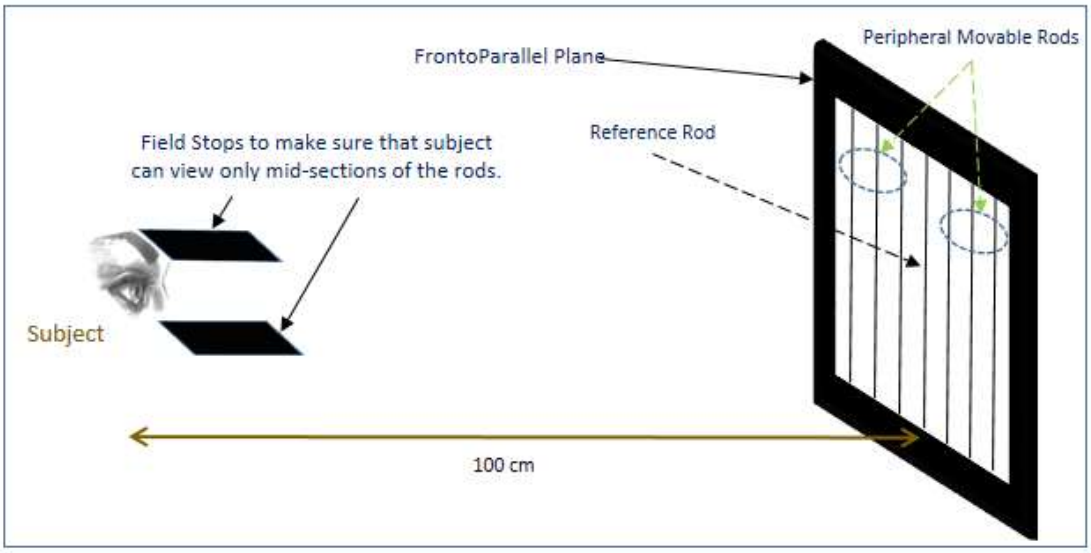

Figure 2.8 Experimental setup to measure the geometry of the perceived vertical fronto-parallel plane: Vertical central reference rod was placed one meter away from the subject. To avoid visual cues, the subject can see only mid-sections of the vertical peripheral rods and reference rod. The subject was instructed to move the peripheral vertical rods (towards or away from him) so that he/she could perceive all the rods in the same fronto-parallel plane.

Change in visual-spatial perception due to Psilocybin-induced hyper-activation was observed in the 16 subjects (six females and ten males, Median Age: 23.5 years). Six vertical rods, three on either side of a central vertical reference rod, were placed in the visual field at 4, 8, and 12 degrees from the pupillary sagittal plane (Figure 2.8). A reference rod was placed one meter away from the subjects. Subjects could see only the middle segments of the rods to suppress any visual cues. They were told to arrange vertical rods in the frontal plane parallel to their face by giving commands to the experimenter to adjust the rods, while keeping their chin and forehead stationary. After the rearrangement of the rods in the parallel frontal plane, the positions of the rods were noted. This study procedure was repeated at 0 (just before ingestion), 90, 180, and 270 Minutes after oral ingestion (psilocybin ingestion: 160 micrograms per kg of body weight). This study method was developed by Fischer et al. (Fischer et al., 1970), who performed the experiment, and we have utilized this empirical data on the transformation of the apparent frontal plane under the effect of the agent, as reported in that paper, so as to do our further analysis, formulation and computation that we present in the sections 2.3.2.

2.3.1.6 Spatial Distortion Threshold Under Hyper-Activation

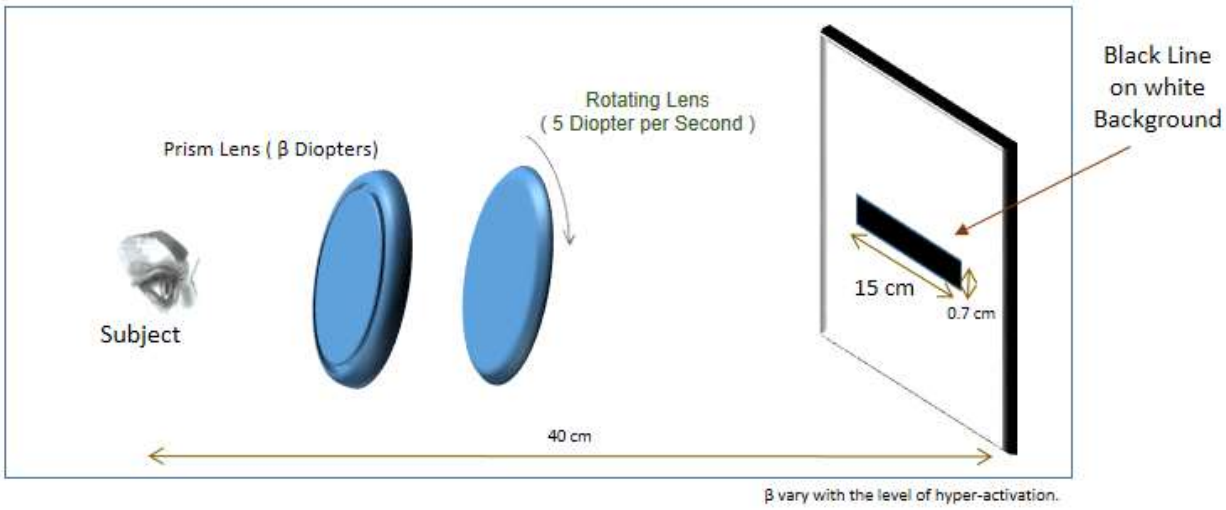

Figure 2.9 Experimental setup to measure the spatial distortion threshold using rotating prism lens: Rotating prism lens introduces the spatial distortion of the thick black horizontal line. The subjects view this black line through two prism lenses. The power of the second lens is kept fixed, while the power of the first lens is increased until the subject can perceive a just noticeable bending distortion in the black line. The spatial distortion threshold is measured by the minimum optical power of the first lens that is required for the subject to perceive the bending distortion.

The spatial distortion threshold in the 15 normal subjects was assessed by finding prism power required for just noticeable distortion of the horizontal 15×0.7 centimeters black line situated at 40 centimeters away from the subject (Figure 2.9). Subjects viewed a black line through a rotating prism (5 prism diopters per second) and a stationary prism. The prism power of a stationary prism was gradually increased until the subject perceived the just noticeable distortion. This procedure was performed at 0 Min (before ingestion), 60, 110, and 280 minutes after oral ingestion of the amount mentioned above of the tryptamine-derivative agent (psilocybin). To paraphrase, the study procedure was formulated by Hill and Fischer (Hill and

Fischer, 1971b) , who performed the experiment, and we have adopted this empirical data on spatial distortion threshold under the effect of the agent as described in that paper, thereby enabling us to develop our original analysis and modeling that we show in the section 2.3.2.

2.3.1.7 Spatial Perception Under Hypo-Activation

The method in the earlier section 2.3.1.6 was adapted for the hypoactivation induced by oral ingestion of 50 milligrams of the phenothiazine-derivative agent (chlorpromazine). The procedure was performed at 0 minutes (before ingestion), 210, and 450 minutes after the ingestion. The spatial distortion threshold for 15 normal subjects was measured using the same experimental setup described in Figure 2.9 of the previous section 2.3.1.6. Accordingly, the experimental methodology was undertaken by Hill and Fischer (Hill et al., 1969), and we have adopted this data on spatial distortion threshold under the effect of the agent as delineated therein, so as to build up our further analysis and formulation that we furnish in the section 2.3.2.

2.3.2 Results

2.3.2.1 Visual Space under the Psilocybin-Induced Hyper-Activation

Subjects under the influence of the psilocybin move vertical rods to perceive them to be on a flat plane; however, they physically positioned them in a substantially curved plane. Under increasing drug influence, the curvature of the curved plane increases further because of the variation in the Psilocybin concentration in the brain. Section 2.3.1.5 may kindly be referred to, where we have mentioned the methodology of the experiment on the transformation of the apparent frontal plane under the effect of psilocybin. We used these data points for curve fitting and thereby formulated the optimal curve, which follows the physical

position of the rods in which the psilocybin action ensues. We find this curve to be a rotated ellipse, whose rotation angle and Gaussian curvature vary with time, as shown in Figure 2.10.

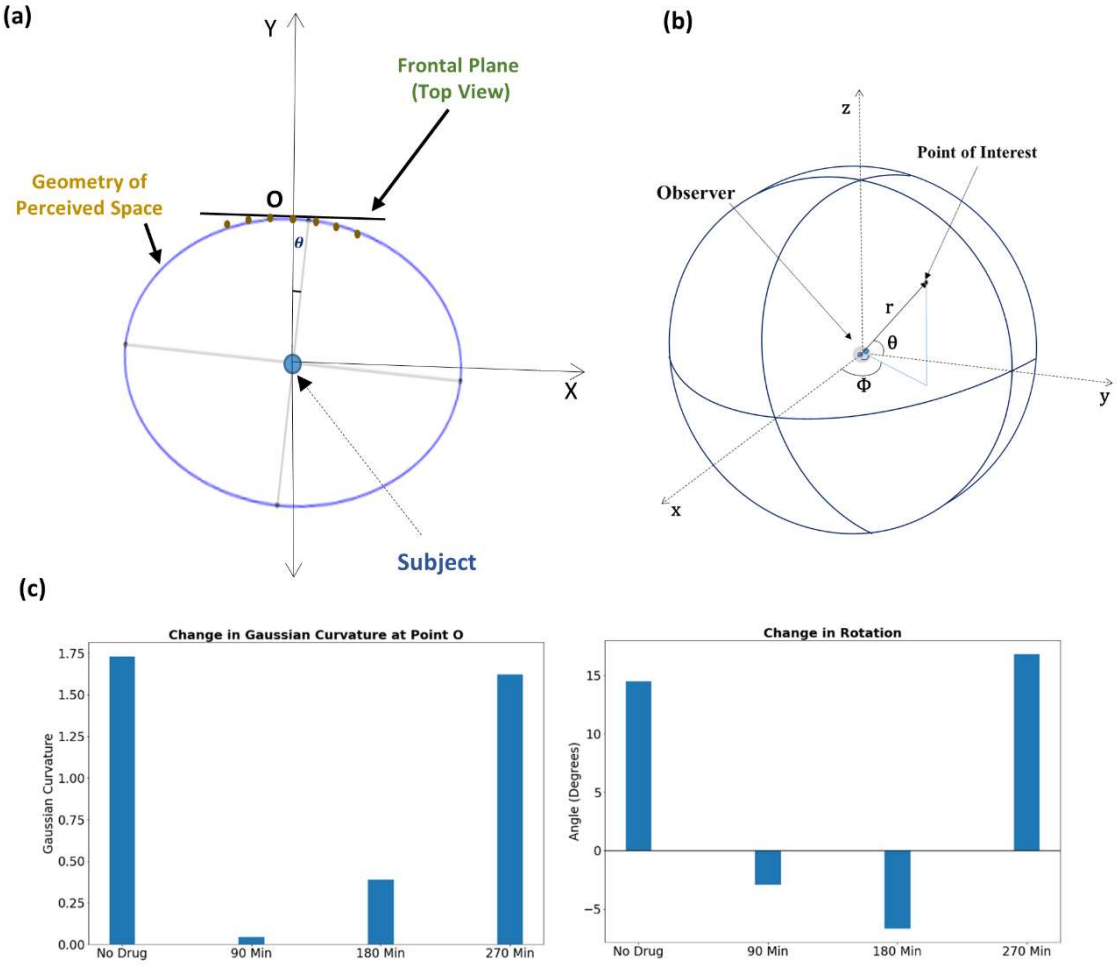

Figure 2.10 (a) Rotated ellipse represents the geometry of the perceived space under psilocybin administration. **(b)** The spherical coordinate system for locating a point in three-dimensional visual space. **(c)** Left panel: Alteration of Gaussian curvature of the perceptual space, the curvature being estimated at the fixation point O. Right panel: Alteration of the rotation angle of the perceptual space, the rotation being estimated from the perspective of the subject at the center of the ellipse. For both panels, the change in the alteration is shown at different time points after psilocybin ingestion.

Using the following procedure, we then derived the metric tensor for the surface of the ellipsoid using the parametric equation (Equations 2.23a, 2.23b and 2.23c) and the transformation of the metric tensor components to the spherical coordinate system (equation 2.24).

The parametric equations for the ellipsoid are:

$$x = a\ cos\,\alpha\ cos\,\beta \tag{2.23a}$$

$$y = b\ \cos\alpha\ \sin\beta \tag{2.23b}$$

$$z = a\ \sin\alpha \tag{2.23c}$$

Tensor transformation equation:

$$g_{\alpha\beta} = \sum_{k=1}^{k=3}\sum_{l=1}^{l=3} G_{lk}\ \frac{dx^k}{dw^\alpha}\frac{dx^l}{dw^\beta} \tag{2.24}$$

In Equation 2.24, G_{lk} are the components of metric tensors in the Cartesian coordinate system, x^i: {x, y, z} coordinates of the Cartesian coordinate system, and w^j:{α, β} coordinate of the point on the ellipsoid. The resultant metric tensor on the surface of the ellipsoid after solving Equation 2.24 is shown in Equation 2.25 below [we used Wolfram Mathematica (Version 11, https://www.wolfram.com/mathematica) for computing the metric tensor]:

$$g_{\alpha\beta} = \begin{pmatrix} \boldsymbol{a^2\mathrm{Cos}[\alpha]^2 + a^2\mathrm{Cos}[\beta]^2\mathrm{Sin}[\alpha]^2 + b^2\mathrm{Sin}[\alpha]^2\mathrm{Sin}[\beta]^2} & \boldsymbol{(a^2-b^2)\mathrm{Cos}[\alpha]\mathrm{Cos}[\beta]\mathrm{Sin}[\alpha]\mathrm{Sin}[\beta]} \\ \boldsymbol{(a^2-b^2)\mathrm{Cos}[\alpha]\mathrm{Cos}[\beta]\mathrm{Sin}[\alpha]\mathrm{Sin}[\beta]} & \boldsymbol{\mathrm{Cos}[\alpha]^2(b^2\mathrm{Cos}[\beta]^2 + a^2\mathrm{Sin}[\beta]^2)} \end{pmatrix} \tag{2.25}$$

where:

α, β: Angular coordinates of the point on the ellipse.

a, b: Length of the semi-major and semi-minor axis.

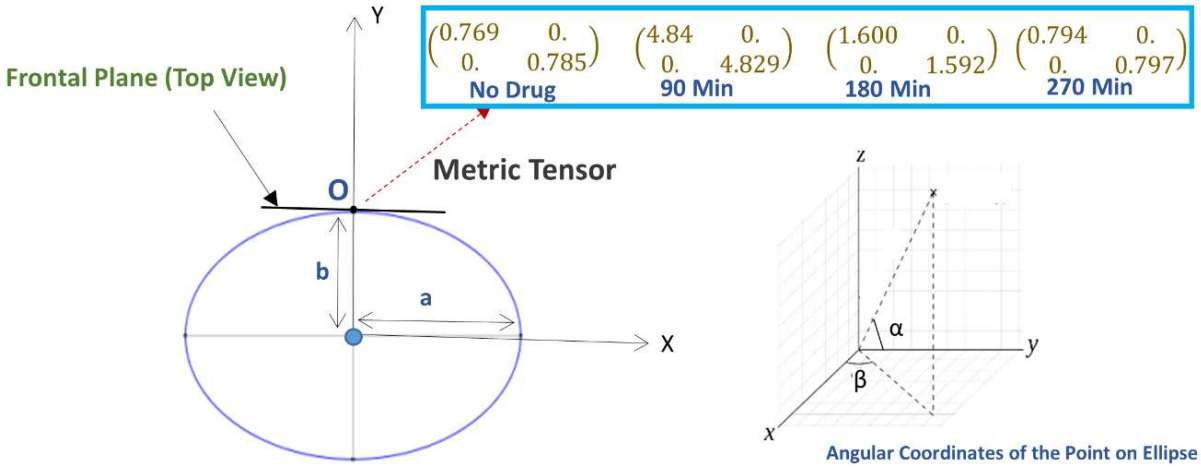

Figure 2.11 *Lower left panel*: The ellipse represents the geometry of the perceived space in the horizontal plane where 'a' and 'b' are the length of the major axis and minor axis (the ellipse is in the horizontal plane). Here, the subject is sitting at the center of the ellipse and looking along the y-axis, i.e., looking directly forward, while sitting in the experimental chair with a chin-rest. Before the experiment starts, the vertical rods are arranged in the vertical fronto-parallel plane. *Lower right panel:* The coordinate system for measuring the angular coordinate of a point on the ellipse. *Upper right panel (Inset box):* The alteration of the metric tensor at point O (fixation point), at four successive time points: time t = 0 (just before the experiment, no psilocybin given), then at time points t = 90, 180, and 270 minutes after psilocybin ingestion.

We applied Equation 2.25 and calculated the change in metric tensor at the subject's visual fixation point O, our results are shown in Figure 2.11. The metric tensor components vary with the time under the psilocybin influence due to variations in the rotation angle, length of the semi-minor axis, and semi-major axis.

2.3.2.2 Relation between Drug Concentration and Perceptual Alterations

Now, we used Equation 2.17 to find out the psilocybin concentration in the brain. Figure 2.12 shows the results obtained after solving Equation 2.17, showing the alteration of psilocybin concentration in brain tissue as time elapses.

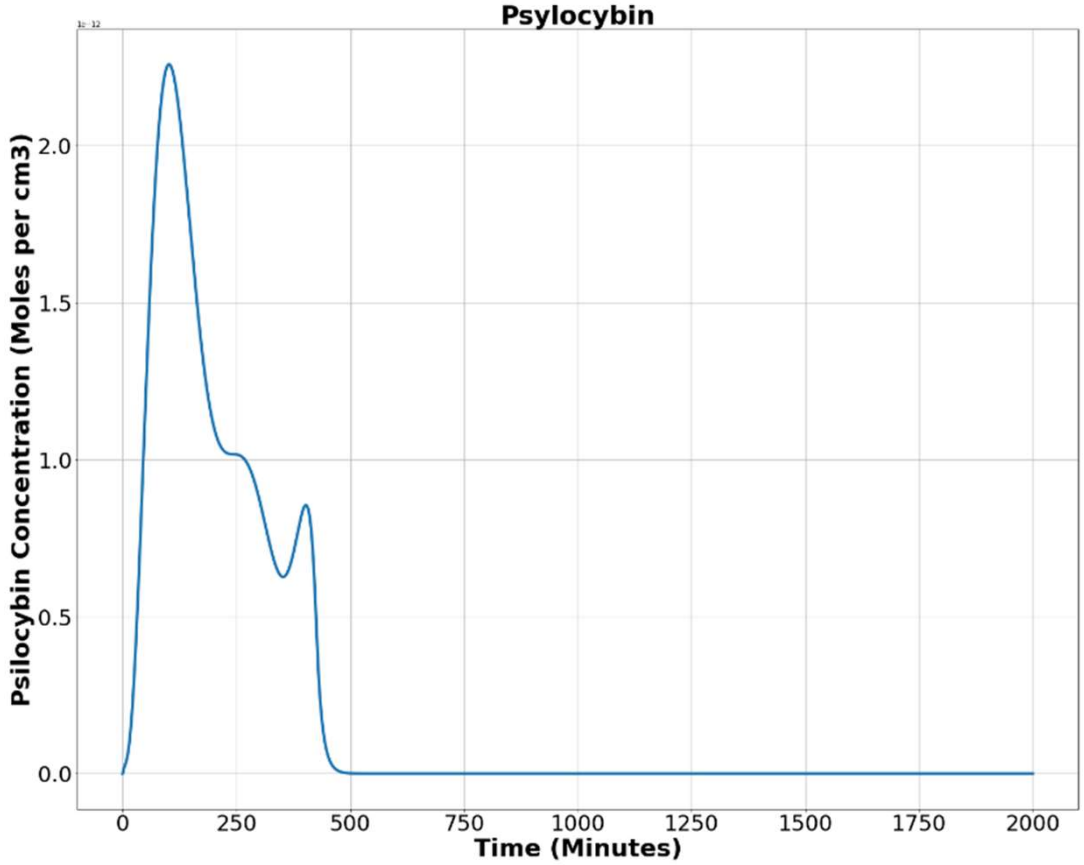

Figure 2.12 Psilocybin concentration in the brain's extracellular space after oral ingestion.

Then, we used the least square method to find the optimum values of the Hill coefficient (**n**) and half-effective drug concentration (**k**), which would be able to satisfactorily predict the metric tensor components using Equations 2.5 and 2.14. This procedure we perform is as follows. First, we calculated the sum of square residuals using (i) the mathematically calculated metric tensor components, using Equations 2.5 and 2.14, and (ii) the experimentally derived metric tensor components (Figure 2.13). Then we plotted the Hill coefficient (n) and half-effect drug concentration (k) against the sum of square residuals, as shown in Figure 2.13(a). As displayed in the two panels of Figure 2.13(a), for **n**=14.8 units and **k**=1.39 picomoles/cm^3, the error between mathematically calculated metric tensor and the experimentally derived metric tensors is minimum, and these two values are thus the optimum values of n and k. We applied this procedure to two diagonal components of the metric tensor and obtained the same results.

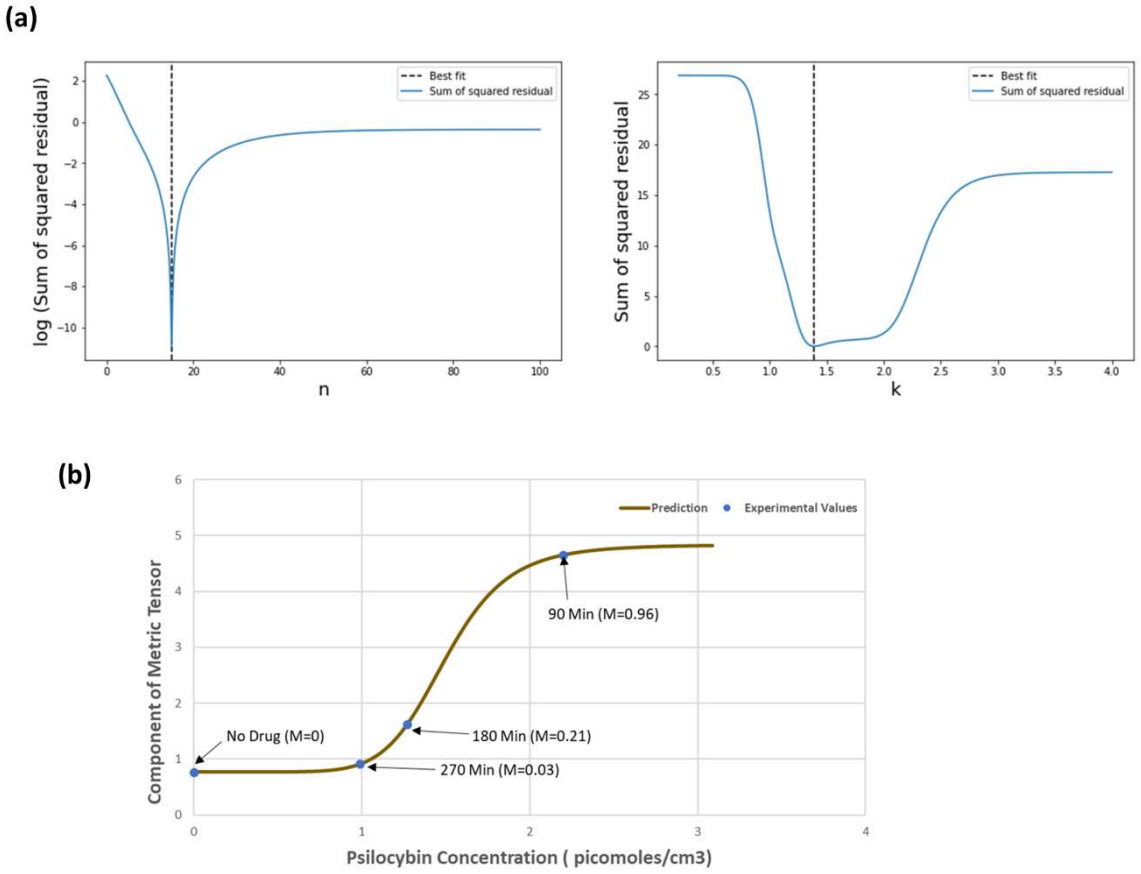

Figure 2.13 (a) Variation of the sum of squared residual with the Hill coefficient (n) and the Half-effect drug concentration (k). At n = 14.8 units (left panel) and k= 1.39 picomoles/cm3 (right panel), the sum of squared residual is minimum, showing the optimum fit. (b) The curve shows the mathematically calculated alterations in the metric tensor component of the perceptual space (solid line) while the Psilocybin concentration changes. The filled circles show the experimentally derived metric tensor components along with the corresponding value of the modulation index (M) and the time duration since the start of psilocybin ingestion (in minutes). Note the close correspondence of the experimental data-points to the theoretical curve. Indeed, the mathematical model is well validated by the experimentally-measured observations, which is further corroborated by robust satisfaction of the goodness-of-fit criterion ($\chi 2$ statistical test firmly satisfied, $p>0.99$).

After calculating the optimum values of the **n** and **k**, we plotted the mathematically calculated value of the metric tensor (the value of both diagonal components were equal) against the experimentally inferred value of the metric tensor (Figure 2.13(b)). As shown in Figure 2.13(b), the experimental data-points closely coincide with the theoretically predicted curve, this coincidence we assessed by the goodness-of-fit statistical criterion (χ2-squared test), which showed that the congruence was very robust ($p>0.99$). This strong congruence thus well validates our computational framework that the temporal alteration of the metric tensor due to psilocybin action follows the temporal trajectory of the modulation index (Equation 2.14). In the next section, we will use these values of **n** and **k** to predict the outcomes of a different experiment.

2.3.2.3 Prediction of Metric Tensor under Psilocybin-Induced Hyper-Activation

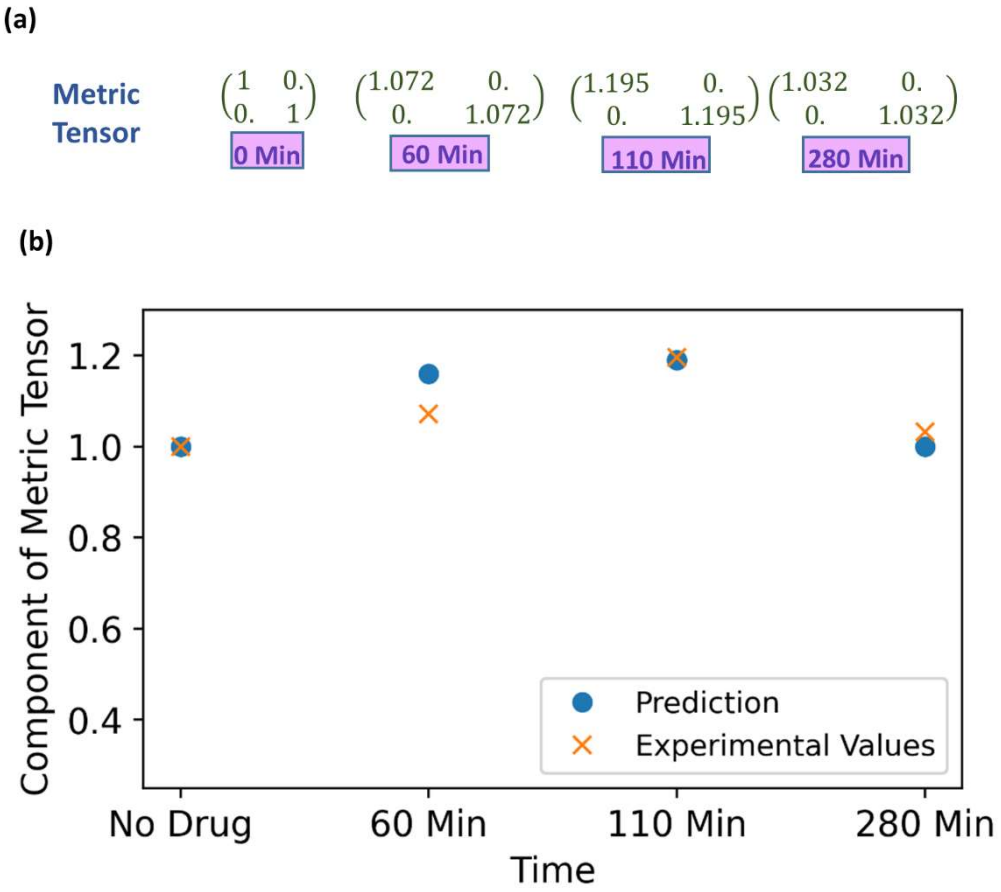

Figure 2.14 **(a)** Metric tensor of the perceived space obtained from corresponding experimentally-measured spatial distortion threshold at four successive time points: time t = 0 (just before experiment, no psilocybin given), then at time points t = 90, 180, and 270 minutes after psilocybin ingestion. **(b)** The metric tensor of perceptual space under the psilocybin induced hyperactivation condition. The theoretically computationally predicted values are shown in blue filled circle, while the experimentally-derived values are shown by the red cross. Observe the strong congruence of the experimental points with the theoretical points. Actually, the theoretical model is soundly validated by the empirical data as substantiated by strong satisfaction of goodness-of-fit criterion (there is robust satisfaction of the χ2-squared statistical test).

To recapitulate, kindly give a perusal on section 2.3.1.6 where we have mentioned the methodology of the experiment on spatial distortion threshold assessed by an optical prism set-up, when the subject is under effect of psilocybin. The prism lens shifts the object's apparent position, and changing the prism power with time introduces visual distortion. However, the brain can counter adapt, and the subject does not perceive any distortion. In that experiment, the counter adaption limit was measured by finding the minimum prism power required to perceive distortions under the psilocybin-induced hyperactivation of the nervous system. Hyperactivation reduces the minimum prism power (β) required to perceive deviation from the straightness of the horizontal black line (Figure 2.9). Variation in the hyperactivation level during the experiment causes different values of β to produce the same perception, which denotes their equivalence in the perceptual space. We find out the physical area covered by the black line for different values of the β. Since the black line covers the same area in the perceptual space, we determine the required change in the metric tensor for the equal area. At the beginning of the experiment, without drug ingestion (at 0 minutes), we can take that the diagonal components of metric tensor are unity, and then we can calculate the metric tensor at time 60, 110, and 280 minutes as follows, the values of the metric tensor that we derived are shown in Figure 2.14(a).

In order to predict the metric tensor components using Equations 2.5 and 2.14, we obtained the psilocybin concentration (C) in the brain at 0, 60, 110, and 280 minutes using Equation 2.17. We used the procedure mentioned in the section 2.3.1.1 to solve Equation 2.17. In previous section (2.3.2.2), we calculated the values of n and k for the psilocybin. Since now we have psilocybin concentration (C), then by using Equation 2.14 and values of n=14.8 and k=1.39 obtained in the previous section, we were able to obtain values of the modulation index

M at 0, 60, 110, and 280 minutes. Thereafter, we derived the components of the metric tensor after applying Equation 2.5 and the modulation index (M) values. A comparison between the metric tensor component obtained from our experimental calculations and from our theoretical model prediction is shown in Figure 2.14(b), and the $\chi 2$ (chi-square) goodness of fit test ($p>0.99$) verifies that the experimental data well validates the theoretically predicted model. Diagonal components of the metric tensor are equal; therefore, only one component is shown in Figure 2.14(b). Hence, our model can satisfactorily predict the metric tensor components.

2.3.2.4 Visual Space under Chlorpromazine-Induced Hypo-Activation

A similar experimental approach was adopted to find the minimum prism power to perceive distortions but after ingestion of the hypoactivation inducing drug chlorpromazine. The details are provided in section 2.3.1.7 which may kindly be referred for recollection. As opposed to hyperactivation, the state of hypoactivation increases the minimum prism power (β) to perceive distortion. We used the same analysis technique (explained in section 2.3.2.3) to compute the metric tensor components for the corresponding prism power, the components of our calculated metric tensor is shown in Figure 2.15(a).

After calculating the metric tensor, we used Equation 2.17 to determine the chlorpromazine concentration in the brain. Figure 2.15(b) shows the results obtained after solving Equation 2.17 for the chlorpromazine. Now, we use a similar procedure like that we used in section 2.3.2.1 for psilocybin. Hence, for chropromazine, we used the least-square method to find the optimum values of the Hill coefficient (n) and half-effect drug concentration (k) for the minimization of the difference between (i) mathematically calculated metric tensor components (using Equations 2.5 and 2.14), and (ii) experimentally derived metric tensor components. We calculated the optimum values of the coefficients n and k. Here, for

chlorpromazine, we obtained the n=50.3 units and k=4.96 picomoles/cc^3. One may observe that n and k are different in chlorpromazine and psilocybin, this reflects the underlying pharmacokinetic and drug potency differences. In Figure 2.15(c), using the n and k values of chlorpromazine, we plotted (i) the experimental values (dots) of the metric tesor, and (ii) the mathematically predicted value of the metric tensor (continuous line).

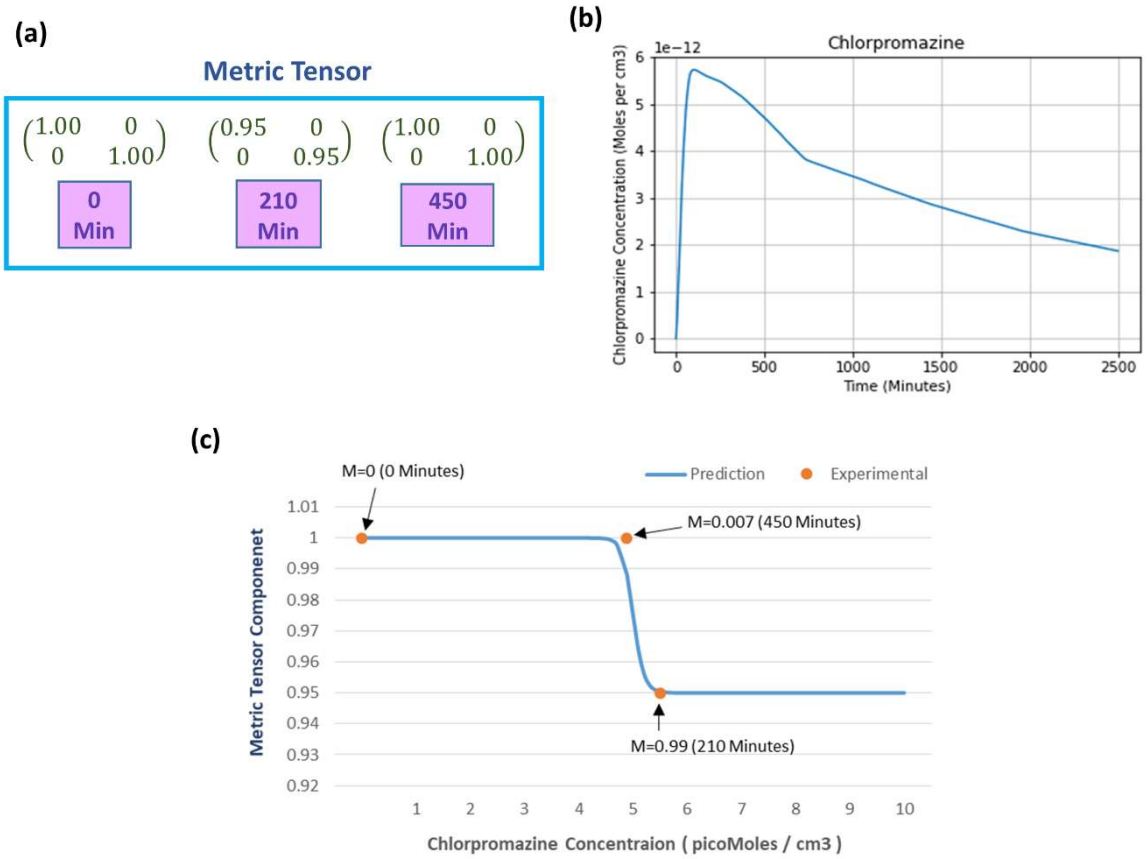

Figure 2.15 (a): Numerical values of the metric tensor components of the perceived space obtained from experimentally-recorded spatial distortion threshold at time t=0, 210, and 450 minutes after ingestion of 50 mg oral intake of chlorpromazine. **(b):** Predicted chlorpromazine concentration (picomoles/cm^3) in the brain's extracellular fluid as calculated from the theoretical computational model (chlorpromazine input is 50 mg). **(c):** The curve shows the predicted alteration in the theoretically computationally formulated metric tensor component of the perceptual space (solid line) while the Chlorpromazine concentration changes. The filled

circles show the experimentally derived data-points estimating the metric tensor components. For each experimental data-point, there is shown the time duration since the start of chlorpromazine ingestion (in minutes). Note the close correspondence of the experimental data-points to the theoretical computational curve. Indeed the mathematical model is well corroborated by the experimentally-measured observations.

From Figure 2.15(c) we observe that the experimentally determined metric tensor components well corroborate the theoretically predicted metric tensor components, as chlorpromazine concentration increases. The close congruence between the experimental data points and the theoretical computational curve in Figure 2.15(c) may be observed. [In parenthesis, it may be mentioned that there are four data points for the psilocybin experiment in Figure 2.13(b), whereas there are three data-points for the chlorpromazine experiment in Figure 2.15(c). It might have been suitable if the chlorpromazine study had also four data points, nevertheless in this experiment with hypoarousal-inducing chlorpromazine, the study logistics afforded the measurement of only three temporal data points on the individual subjects]. Note that Figure 2.15(c) shows a sigmoid-type decreasing curve for chlorpromazine, and the pattern is reciprocal to Figure 2.13(b) that displays a sigmoid-type increasing curve for psilocybin. This reciprocity is a manifestation of the neurophysiological complementarity between chrorpromazine (hypoactivation agent) and psilocybin (hyperactivation agent).

2.3.2.5 Anatomical Connectivity between the Entorhinal Cortex and Area V2

2.3.2.5.1 Three Tesla MRI

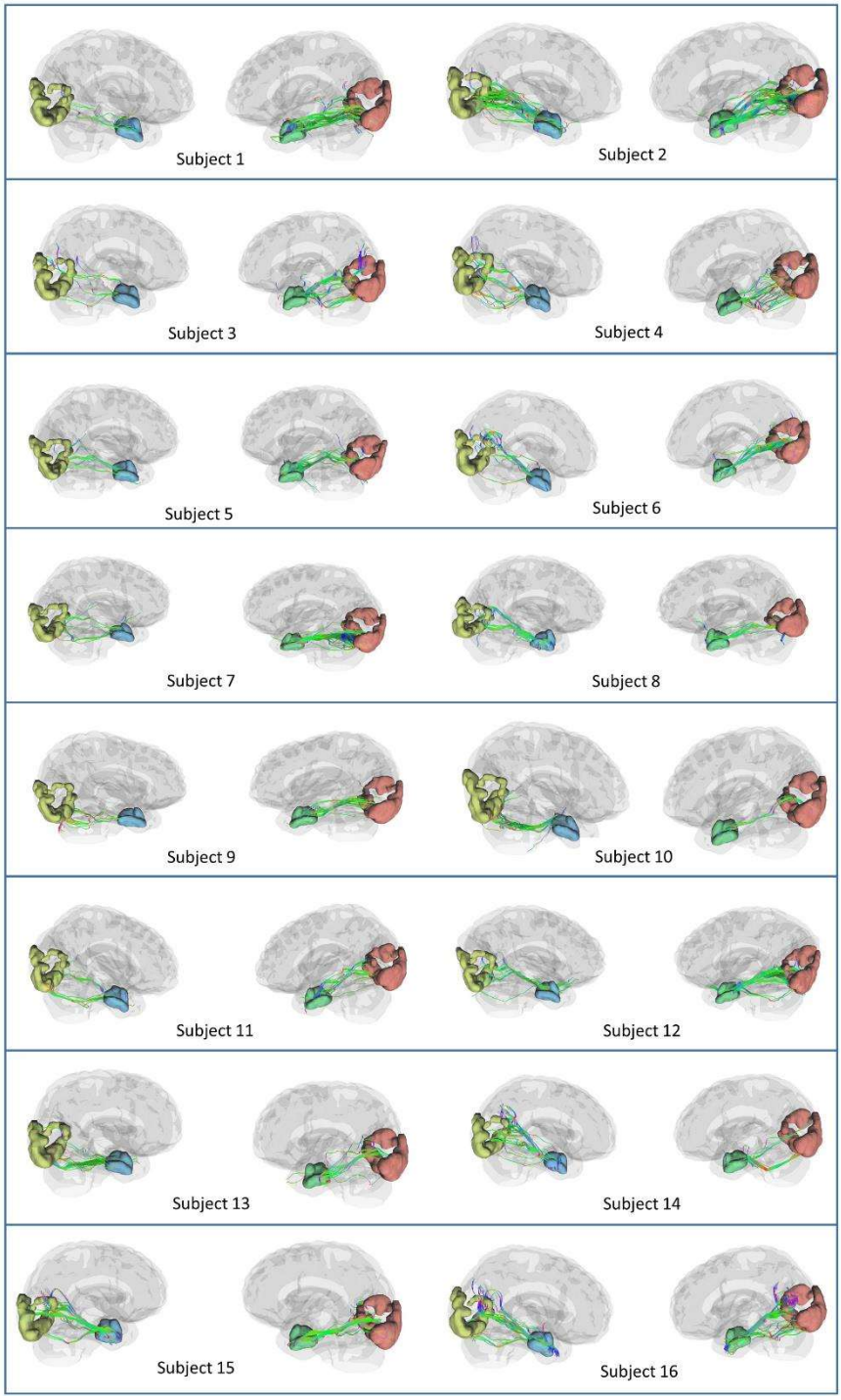

Figure 2.16 Anatomical connectivity (neural tracts) between the entorhinal cortex and visual cortex (area V2) in the sixteen subjects obtained after performing the tractography experiment.

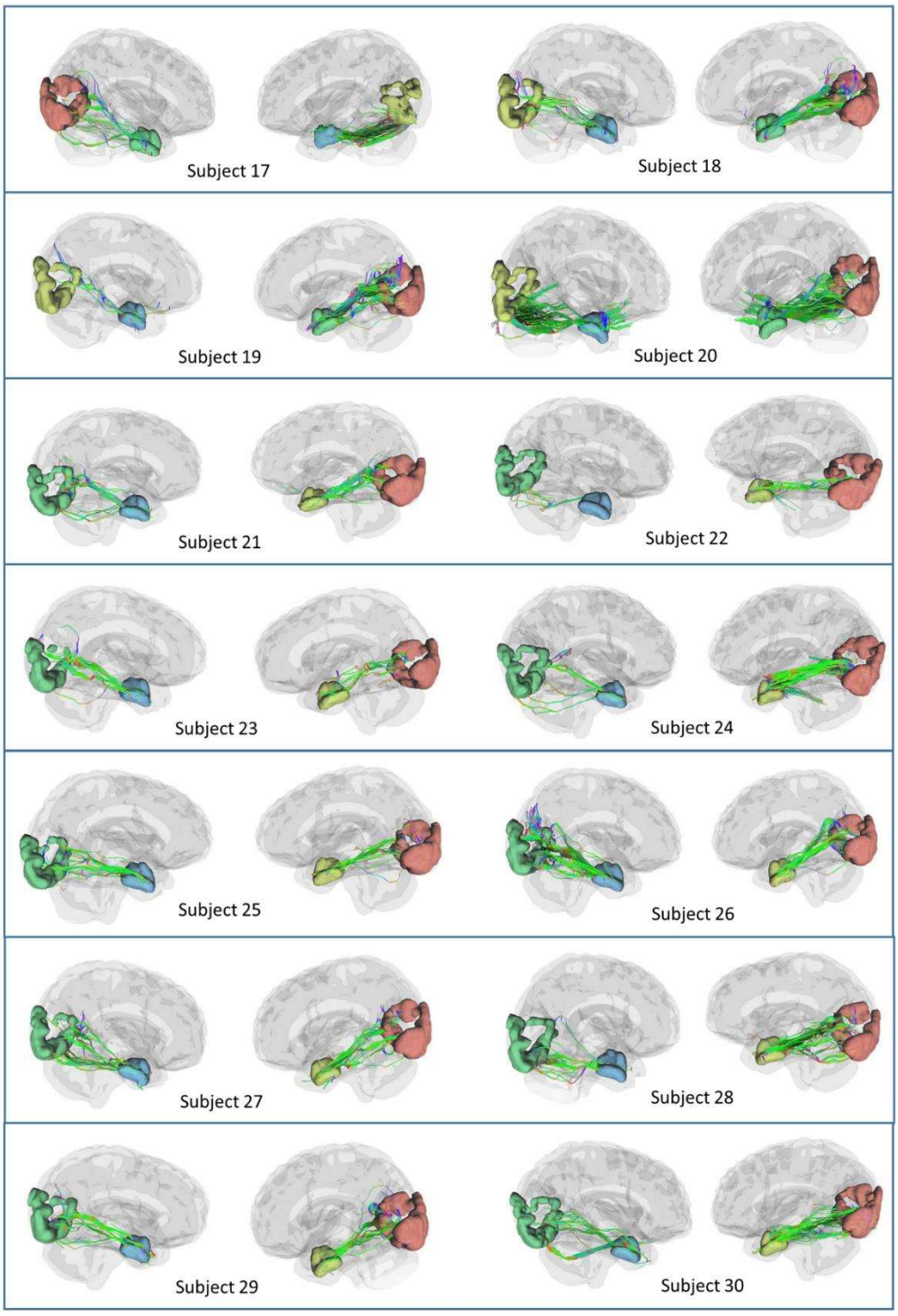

Figure 2.17 Anatomical connectivity (neural tracts) between the entorhinal cortex and visual cortex (area V2), obtained from MRI-tractography analysis of the fourteen subjects (Subject 17 to 30).

Table 2.1: Different parameters related to the neural tracts obtained between the entorhinal cortex and area V2.

Parameters	Left Hemisphere	Right Hemisphere
Mean length (mm)	116.8 ± 4.43	118.5 ± 5.42
Fractional Anisotropy	0.2921 ± 0.04	0.2784 ± 0.03
Mean Diffusivity	1.086 ± 0.12	1.1531 ± 0.15
Axial Diffusivity	1.4013 ± 0.13	1.4572 ± 0.17
Radial Diffusivity	0.9375 ± 0.13	1.009 ± 0.15

Based on the theoretical and experimental studies, we have sketched a framework for a grid cell-like encoding of the perception related to various sensory modalities (Figure 2.5). Indeed, grid cells are experimentally recorded from area V2 (Long et al., 2021). Since the current study focuses on visual-spatial perception, we performed a MRI tractography experiment to find the anatomical connectivity between the entorhinal cortex and visual area V2 to verify our formulation and observation. Using the methodology explained in section 2.3.1.3, we conducted diffusion MRI scan-based tractography for thirty normal subjects. The tracts obtained after analyzing the diffusion MRI scan are visualized in Figure 2.16 for 16 subjects, and tracts of the remaining 14 subjects are shown in the Figure 2.17 of the supplementary materials. Results distinctly depicted the presence of the neuronal pathways between the entorhinal cortex and area V2 in all 30 subjects. The quantitative parameters related to the neural tracts are shown in hemisphere-wise in the Table 2.1. The tractography results provide evidence of the anatomical connectivity between the entorhinal cortex and visual cortex (area V2), thus supporting our theoretical formulation.

2.3.2.5.2 Seven Tesla MRI

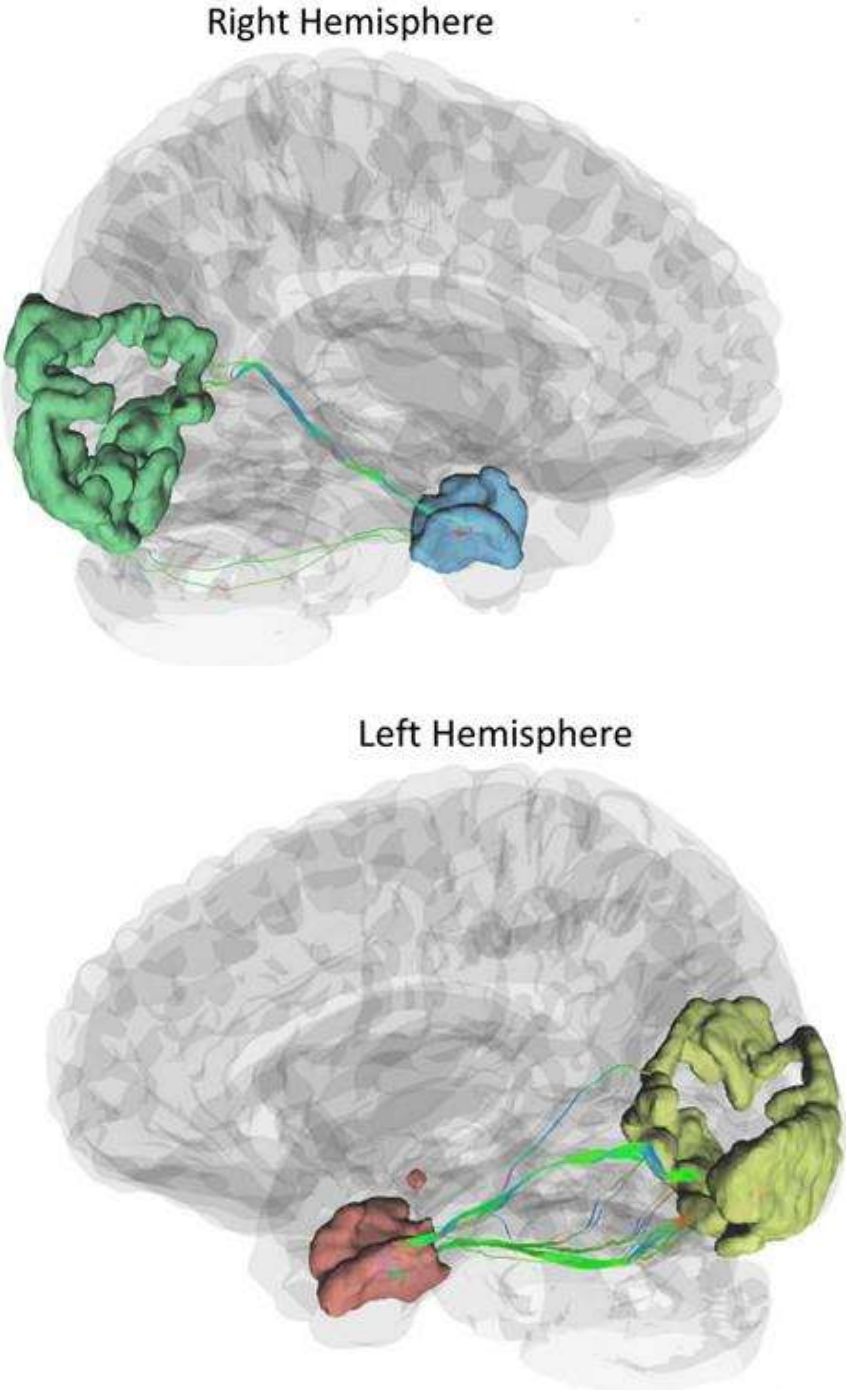

Figure 2.18 Anatomical connectivity (neural tracts) between the entorhinal cortex and visual cortex (area V2), obtained from MRI-tractography analysis of the 7 Tesla diffusion MRI scan. (Cognitively normal, female, 27 years)

We also examined a 7 Tesla diffusion MRI scan to see if our results hold up when using a different strength MRI machine. We looked at the connections between area V2 and the entorhinal cortex. The results are shown in Figure 2.18. The results clearly show that there are pathways between the entorhinal cortex and area V2.

2.3.2.6 Grid Cell Activity under Drug-Induced Perceptual Alterations

We have delineated the role of the grid cell-like representation of visual spatial perception in section 2.2.4 based on various experimental and computational studies. Here, we constructed a neuronal network model of the grid cells (see section 2.3.1.4 for details) and simulated the modulatory effect of the drug molecules. We calculate the grid cell activity alterations under normal (no drug) and drug-induced activation conditions; the results are shown in the following subsections.

2.3.2.6.1 During Normal Conditions (No Drug Condition)

Under no drug condition ($\Delta I = 0$), we calculated the activity of the nodes for the 4 seconds (time step=0.01 second) for the following cases: (i) Eyes fixating in a visual field (E(t)=0) (ii) Eyeballs constantly moving (E(t)=constant) (iii) Random movement of the eyes (E(t)=random). Figure 2.19 shows the results after the simulation. When eyes are not moving (fixating), the few nodes are constantly active independent of the time (Figure 2.19(a)), thereby showing the attractor dynamics of the neuronal network. However, the activity of the nodes varies with time (Figure 2.19(b) and 2.19(c)) during the eyeball movements. When eyeballs are moving with constant speed, the periodic activation of the nodes is apparent. However, in the case of random movements, the activity of the nodes seems random with time.

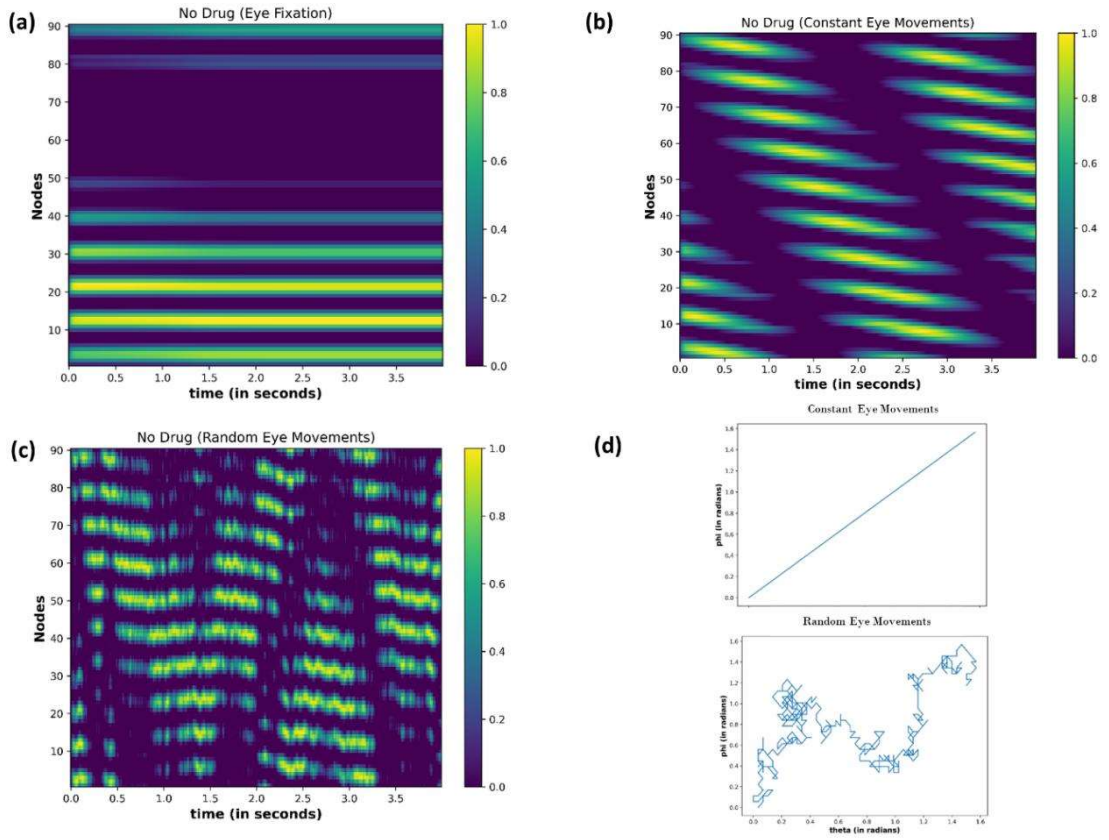

Figure 2.19 Activity of the neuronal nodes under no-drug condition (a) when eyes are not moving and fixating in the visual field (b) when eyes are making a constant movement in the visual field (c) when eyes are randomly scanning in the visual field. (d) Variation in the angular position of the eyeball movements during constant eye movement (upper) and random eye movement (lower).

2.3.2.6.2 Under Drug-Induced Neural Activation

We found out the effect of the drug-induced neural activation on the grid cell activity by changing the △I from 0 to 0.30. △I=0 is equivalent to the no drug condition, and non-zero values of the △I represent the drug-induced activation. We simulated the neural network model of the grid cells for 4 seconds (time step: 0.01). Similar to the no-drug situation, we evaluated the network activity in three cases (eye fixation, constant eye movements, and random eye movements); the results are as follows:

(i) *Eyeballs fixation (no eye movement):* Figure 2.20 shows the node activity under different △I values**.** Because eyes are not moving, a few nodes are constantly active for different values of the △I (Figure 2.20a)**.** However, different sets of nodes are active as the △I changes (Figure 2.20b). These observations indicate that the neuronal coding of the visual spatial perception is changing as drug-induced neural activation (△I) varies.

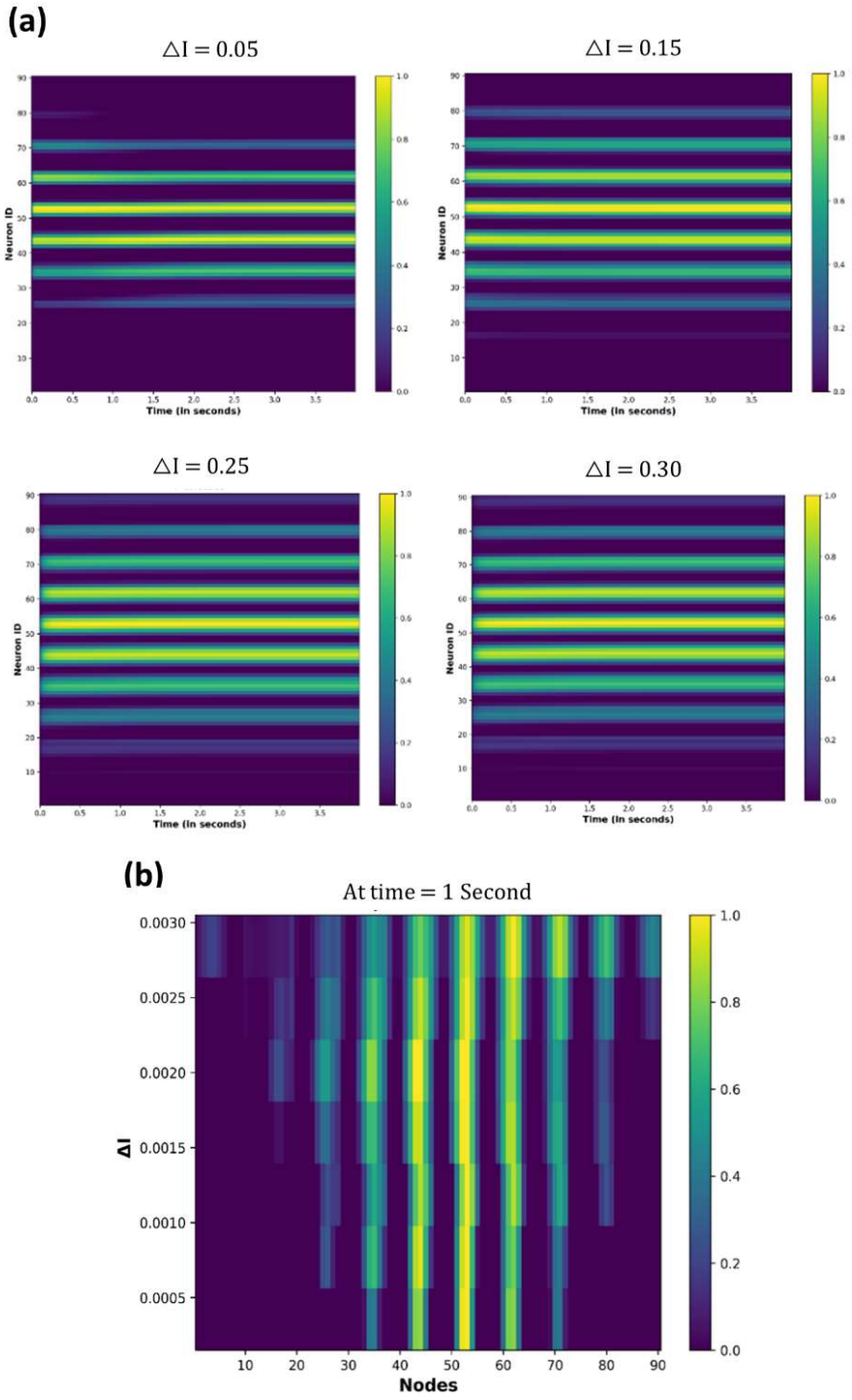

Figure 2.20 Activity of the neuronal nodes under drug-induced activation (Eye fixation): (a) Activation pattern of the nodes under the different values of the △I=0.05, 0.15, 0.25, and 0.30. (b) Variation in the activity of node number 47 as the △I changes from 0 to 0.30.

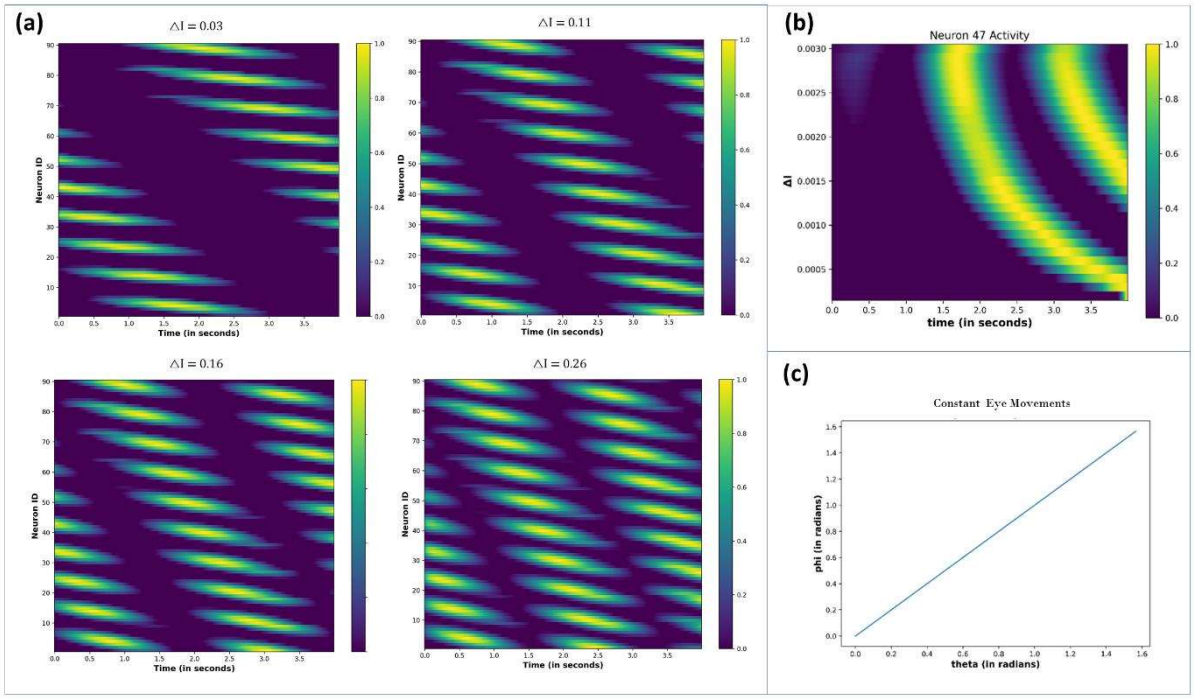

Figure 2.21 Constant eye movement under drug-induced activation: **(a)** Change in the periodic activation of the neuronal nodes for different values of the △I. **(b)** Activity of the neuronal node 47 for the different values of the △I and time. **(c)** Variation in the angular coordinates of the moving fixation point. At the origin, t=0 second: θ=0 and Φ=0; thereafter, θ and Φ are increasing linearly with time, indicating that eyes move with a constant velocity across both angular directions.

(ii) *Constant eye movements:* Figure 2.21 shows the neural network activity under different values of the △I. The nodes show periodic activation, whose period decreases as the △I increases (Figure 2.21a). Thus, the neural activation affects the firing pattern of the nodes, as highlighted in Figure 2.21b, by showing the variation in the activity of node 47 as the △I changes.

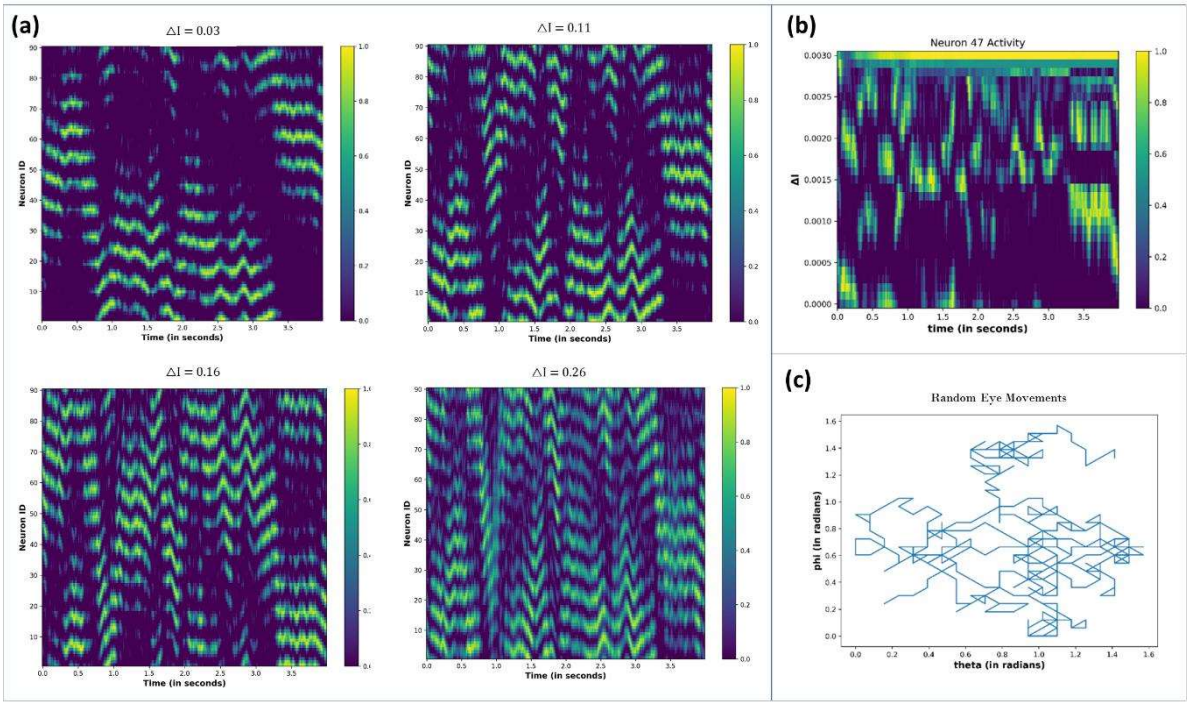

Figure 2.22 Random eye movement under drug-induced activation: **(a)** Activity pattern of the neuronal nodes for the different values of the ΔI, as the eyeball is moving randomly in the visual field. **(b)** Temporal variation in the activity of neuronal node 47 for the different values of ΔI. **(c)** Variation in the angular coordinates of the randomly moving fixation point.

(iii) *Random Eye movements:* When the eyeballs randomly scan the visual field, the resultant network activity is shown in Figure 2.22. Contrary to Figure 2.21, the periodic activity of the nodes is not visually observable. However, as the ΔI increases, temporal variation in the node activity becomes prominent (Figures 2.22a and 2.22b).

2.3.2.6.3 Quantification of the drug-induced neural activation

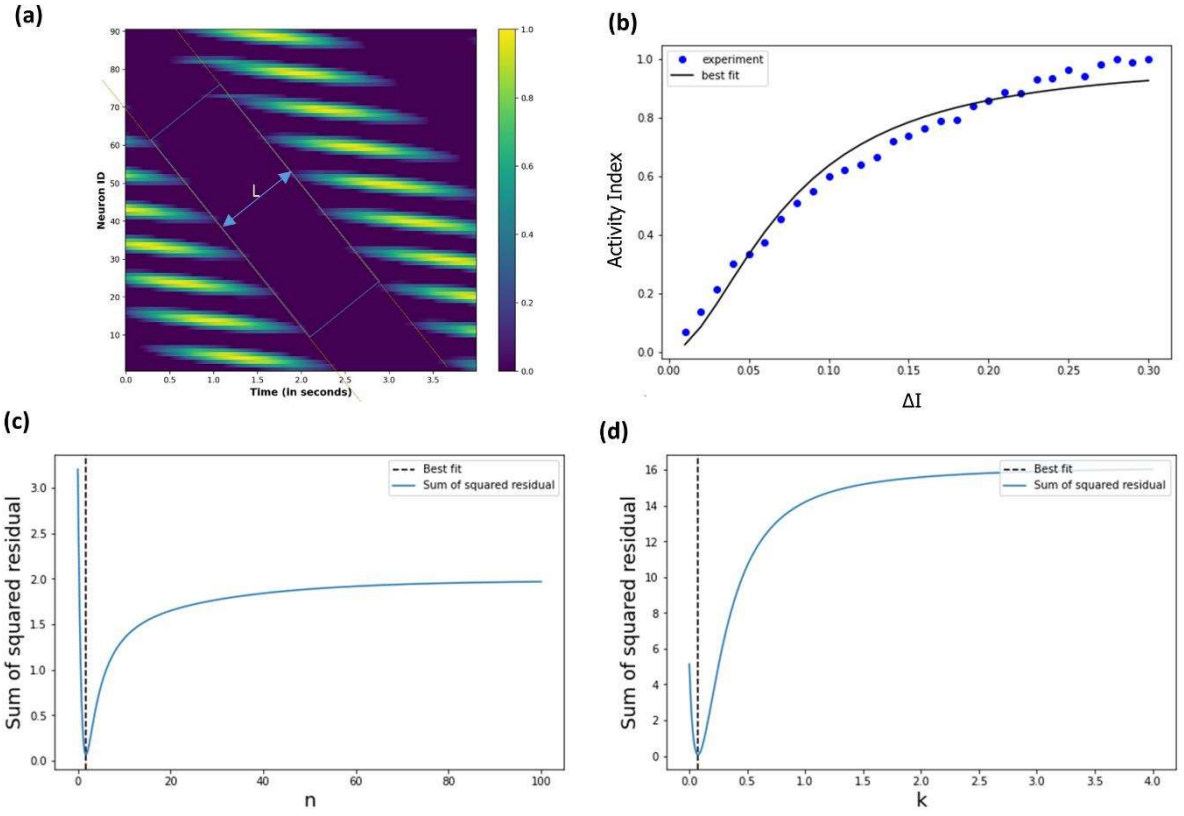

Figure 2.23 (a) Spatiotemporal distance (L) for a particular value of the ΔI. We calculated L for the different values of the ΔI. **(b)** Experimentally calculated activity index (filled circles) using the neural network-based model of grid cell network model, and the corresponding Hill equation curve is also shown. **(c) & (d)** Variation of the sum of squared residual with the Hill coefficient (n) and k. At n=1.8 and k=0.07, the sum of squared residuals is minimum and optimally fits the observed data points.

In the previous subsection (2.3.2.6.2), we showed modulation of the grid cell activity due to altered neural activation ($\triangle$I). In order to quantify the modulatory effect of the drug molecules, we considered the simple case of constant eye movement during which the nodes showed periodic activity (Figure 2.21a). Figure 2.21a shows the spatiotemporal activity of a grid cell network. We measured the distance (L) between the periodic activation of the nodes

using MATLAB's Image Viewer tool (Mathworks Inc.) for the different values of the △I, as shown in Figure 2.23a [the values of *L* changes, as △I varies, as shown in Appendix-A]. Thereafter, we defined an activity index (AI) for quantifying the modulation of the grid-cell network activity, such that the value of the AI ranges between 0 to 1, whereby the AI can be delineated as in Equation 2.26 below, where L_{max} is the maximum value of the L:

$$AI = 1 - \frac{L}{L_{max}} \tag{2.26}$$

Thence, we calculated the activity index (AI) for each value of the △I, whereby we obtained the data points (filled circles) in Figure 2.23b. It is evident that the pattern of these points is a saturation function, and so we explored whether these points follow a Hill equation. Then, we used the least square method to fit the variation in the activity index (AI) with the following Hill equation:

$$AI = \frac{1}{1 + \left(\frac{k}{\triangle I}\right)^{n}} \tag{2.27}$$

Thereby, we obtained the optimum values of the Hill coefficient (**n**)=1.8 and **k**=0.07, the curve of this equation is drawn in Figure 2.23b. We note the close correspondence between the data points and the Hill equation curve (the $\chi 2$ test is well satisfied, with $p > 0.98$). Figure 2.23c and 2.23d show the sum of squared residuals for different values of **n** (Hill coefficient) and **k** respectively, and elucidates that for n=1.8 and k=0.07, the sum of squared residuals is minimum for which the Hill equation optimally fits the data points (filled circles) of the activity index, AI, in Figure 2.23b.

Now, we recapitulate the modulation of visual perception under pharmacological action [Equation 2.14]. To recollect, the modulation index (M) represents the modulatory effect of drug-induced activation on visual-spatial perception. As shown in Equation 2.14, the Hill equation there shows the mathematical relationship between the modulation index (M) and the drug concentration (C), which we are re-writing as follows:

$$M = \frac{1}{1 + \left(\frac{k}{C}\right)^{n}} \tag{2.14}$$

Let us give attention to the two formulations of the Hill equation, namely (i) Equation 2.14, which delineates how rising drug concentration (C) increases the modulation index (M) that becomes gradually saturated, and (ii) Equation 2,27, which shows that as the interaction index (△I) increases, there is a rise in the activity index (AI) which gradually saturates. In other words, Equation 2.27 can be taken as that when the drug-induced interaction rises, then there is a gradual increase in the neural network activity. Thus, we see the close equivalence between Equations 2.14 and 2.27, both describing the effect of the drug on the neural system from two perspectives: (a) Equation 2.27 describes the perceptual changes at the neuronal network dynamics level, while (b) Equation 2.14 describes visuospatial changes at the perceptual-behavioral level (see the last paragraph of sec. 2.2.2). In other words, the Hill model can unitarily elucidate visuospatial changes with neuromodulatory chemicals across scales, i.e., neuronal level and behavioral/perceptual level.

2.4 Discussion

2.4.1 Quantitative Model

As per the ecological approach to psychological dynamics, the central nervous system furnishes as a perception-action system, whereby the neural system cognizes the surroundings and acts on or adapts to the environment, so as to optimize the integrated functioning of the organism. The sympathetic and parasympathetic nervous system controls the human body's response to external situation, which is necessary for survival and homeostasis. However, this also manifests in the change in the organization and comprehension of sensory information, termed as perception. We focused on visual perception in this study, although our methodology can be extended to other sensory modalities. Since it is not easy to experimentally quantify and control naturally induced hyperactivation and hypoactivation of the central nervous system (e.g. stress or stupor), we focused on the pharmacologically-induced hyper or hypo-activation, which is quantifiable and controllable based on the dosage amount.

We devised a mathematical coefficient: the modulation index (M), whose value can vary between 0 and 1. The modulation index is a single parameter representing the perceptual alterations due to the neuropharmacological action. We elucidated that the activation level (i.e., dose amount) and perceptual alteration (i.e., modulation index) are related to each by the Hill equation (Equation 2.14), since perceptual alterations occur due to the biochemical process between drug molecules and receptors. We formalized the metric tensor characterizing the geometrical properties of the visual space, and defined how these metric tensor components will vary with the modulation index (M) (in Equation 2.5). Hyperactivation and hypoactivation conditions cause perceptual deviations in opposite directions, as shown by the arousal index μ being +1 and -1, respectively, for hyper and hypo-activational drugs. Further, the intensity of

the perceptual distortion depends on the individual's tolerance to the drug as characterized by the personalized weber constant P (Equation 2.5 shows the incorporation of both parameters μ and P). We quantify the level of hyperactivation and hypoactivation by initially formulating a differential equation (Equation 2.17) describing the spatiotemporal dynamics of the drug in the brain. Thereafter, we calculate the temporal variation in the metric tensor of the visual space after the oral ingestion of the psilocybin (hyperactivation inducing drug). Thence, we find out the value of the Hill coefficient (n) and half-effective drug concentration (k) (Equation 2.14), using experimental observations on psilocybin administered subjects.

2.4.2 Verification by Empirical Finding

Moreover, drugs, even if they stimulate the same type of activation pathways, may have different bioavailability and biochemical reaction dynamics. Therefore the value of n and k may vary with different drugs. Then, we applied the above-derived values of the Hill coefficient (n) and half-effective drug concentration (k) to a different experimental investigation measuring the spatial distortion threshold under psilocybin action. We predicted the metric tensor at different time points using Equations 2.5 and 2.14. Indeed, we found out that the experimental values well validate our prediction. To corroborate this validation, the statistical goodness-of-fit assessment (χ2-test) was performed, and the corroboration was calculated to be really strong. Using a similar methodology, we found the values of the Hill coefficient and half-effective drug concentration for another different experiment, which involved assessing spatial perceptual distortion under the hypoactivation inducing drug, chlorpromazine. The theoretical prediction curve was also closely substantiated by the experimental data points.

2.4.3 Practical Perspective:

In our study, we tested our mathematical model using experiments involving psilocybin and chlorpromazine. However, it is known that other drugs can also impact visual perception. For instance, methamphetamine stimulates the sympathetic nervous system and affects visual attention and sensory processing. Hedger et al. used functional magnetic resonance imaging (fMRI) to study the effects of methamphetamine on healthy adults and found that methamphetamine increased activation in certain areas of the visual association cortex when participants viewed less complex images (Van Hedger et al., 2019). This suggests that methamphetamine might boost higher-level sensory processing and visual attention for simpler stimuli.

Similarly, MDMA, another drug that stimulates the sympathetic nervous system, can alter visual perception processes related to serotonin functions in the occipital lobe (White et al., 2013b). This could be due to impairment to the serotonin system, affecting visual processing. Drugs that activate the parasympathetic nervous system, like cholinergic agonists, also affect visual perception (Kunnath et al., 2023). Vagal nerve stimulation, which activates the parasympathetic nervous system, can influence both top-down and bottom-up visual perception (Park and Thayer, 2014). Drugs like donepezil, which mimic the actions of the parasympathetic nervous system, may improve visual abilities by enhancing information processing in the primary visual cortex through acetylcholine modulation (Soma et al., 2013). Our mathematical framework can be used to analyse the visual perception alteration by above mentioned drugs by updating the drug dependent variables in the equations to account for their specific effects.

Our various types of experimental validation proved that the variations in the geometry of the visual space due to the modulation of the neural activity (due to the pharmacological agent) could be precisely mathematically modeled using our formulations. In our approach, we used the drug concentration in the brain as an indicator of the neural activation level, the pharmacological activity follows the Hill equation and modulates the perception. We also need to extend the applicability of activation-induced spatial distortion to the practical consequences of altered activation due to environmental or endogenous factors, such as stress, bipolar conditions, stupor, or depressive affect. Therefore, applying our model to the application-oriented scenario would be very useful. For this, there should be a parameter that denotes the activation level (similar to the drug concentration in the brain at any moment), and the parameter should vary with time according to the activation level. A suitable candidate for this parameter is the quantitative variability index in the EEG signal, such as Goldstein's coefficient of variation (G) across different frequency bands (Fischer, 1971; GOLDSTEIN, 1978). In addition to finding a suitable parameter denoting the activation level, the relationship between the drug-induced perceptual modulation index (M) and he activation level parameter G needs to be formalized, derived, and approximated.

2.4.4 Neuron-Level Processes:

We provided a grid cell oriented framework to account for a possible underlying neuronal principle behind the modulation of visual space geometry due to drug-induced autonomic nervous system activation. Our analysis indicates that the local spatial map at the visual cortex and global spatial map at the entorhinal cortex is represented by the grid cells at the neuronal level. As verified and highlighted by our MRI-tractography experiment, the entorhinal-hippocampal network is anatomically linked with the visual cortex (area V2),

thereby may be enabling the integration of sensory information with prior knowledge (memory), so as to encode different positions in the visual space. We indicated that nervous system activation alters the interaction between the grid cells in the network, inducing changes in the metric representation of the physical space into the perceived space.

Various computational models of the grid cells have been developed over the years (McNaughton et al., 2006; Guanella et al., 2007b; Burak and Fiete, 2009a), and based on these models, we constructed and simulated a grid cell network under the drug action. The simulated action of the drug molecules altered the grid-cell firing characteristics, thereby indicating the modification of the neuronal representation of the external visual field, which may manifest as the modulation of the visual-spatial perception. We devised a new parameter (activity index) to quantify the changes in the activity of the grid cell network and found that the activity index (AI) also follows the Hill equation (similar to the modulation index in Equation 2.14). Using the neuronal network model of the grid cell network, we showed that the drug-induced alterations in the visual spatial perception follow the Hill equation as predicted by our mathematical formulation.

2.4.5 Spectrum of Perceptual Modulation:

Our model provides the computational foundation, validated by the independent experimental observation, of quantifying the perceptual alteration due to the altered neural activation. In other words, our study specifies a quantitative deviation compared to the baseline perceptual levels, which correlates with the cerebral arousal level. Here, we focus on the visual system and show that the metric tensor of the perceived geometry can vary, which manifests as variations in visual assessment, its distortion, and, accordingly, the subject's gauging of the environment. In principle, we showed that grid cell like neuronal representation map perceived

visual space and pharmacological agents affect the grid cell firing characteristics resulting in the modulation of the visual-spatial perception. Additionally, our model has an incisive potential to apply to the most general case of the naturally occurring variations in cerebral arousal, either hyperarousal states as stress, or hypoarousal states as trance. Indeed, we have indicated that our approach can also be applied to arousal-induced distortion of perceptual space of different sensory modalities, such as visual space, auditory space, olfactory space, and sensory-motor space.

A primary rationale for the applicability of our framework to multimodal sensory systems is that grid cells-like neural representations exist while navigating in the visual space, olfactory space, auditory space, and sensorimotor space, this implies a general nature of the grid cells to represent cognitive maps being generated from different types of the perceptual modalities. Our quantitative predictive model to forecast perceptual distortion and altered judgment may provide a novel approach to assessing and improving human performance. In high-stress professions such as aircraft pilots, submarine navigators, and spacecraft astronauts, high arousal can often induce hyperactivation and cause an error of judgement and mishap due to changes in visual perception or auditory perception (Wiegmann et al., 2005; Harris, 2016). By measuring the cerebral arousal level, one can devise an algorithm and alarm to give feedback to the human operator to avoid accidents.

2.4.6 Biomedical Implications:

Using the reverse approach, experimental measurements of the metric tensor (such as by measuring handwriting alteration) can be used as a novel, rapid, inexpensive paper/pencil behavioral-psychometric test to assess the level of cerebral arousal, thereby detecting and

monitoring depressive disorders (hypoactivation) or manic disorders (hyperactivation), or their alternating combination, as a cyclothymic disorder. It is also known (Fischer, 1967) that mood disorders, such as bipolar psychosis, produce respectively expansion and contraction of the spatial area of handwriting during the manic phase and the depressive phase. This cited investigation (Fischer, 1967; Nolen et al., 2020) has highlighted that the bipolar disorder of the artist Van Gogh can be well-mapped and analyzed in terms of the geometric alteration in his art and handwriting as time progressed. Indeed, our proposed aforesaid behavioral testing has considerable potential to be used as a ready economical biomarker to monitor the therapeutic effect of clinical interventions on bipolar or mood disorder patients. Such behavioral testing can be utilized on a day-to-day basis for close monitoring and can supplement invasive blood-based biomarkers (García-Gutiérrez et al., 2020) to check the effects of the psychiatric drugs administered; indeed, intravenous blood-based biomarkers may not often be measured on a day-to-day basis.

Further, visuospatial tests to measure the metric tensor components of the perceived space may be designed, and a readily affordable planimetry-based test may be developed to measure the handwriting area at different times. Recent *in silico* models of neuropsychiatric patients and therapeutic intervention optimization are available to assess behavioral therapeutic approaches (Hoffman et al., 2011; Huys et al., 2021). Hence, it may be indicated that our mathematical spatiotemporal analysis could improve the existing available neuroinformatics models of simulated patients for developing more precise quantitative computational models of neuropsychological disorders. As large electrophysiological datasets, genomic maps, and digital therapeutic records become readily available, it may be worthwhile to develop in-silico models of behavioral, and neuropsychiatric effects and their alteration by clinical interventions.